# MEMBER

# REPORT

# [*China*]

ESCAP/WMO Typhoon Committee
17th Integrated Workshop
(Video conferencing)
29-30 November 2022

# CONTENTS

# I. Review of Tropical Cyclones Affecting China since Last Session of ESCAP/WMO Typhoon Committee

## 1.1 Meteorological and Hydrological Assessment

Following the end of last La Niña event which occurred from August 2020 to April 2021, the sea surface temperature anomaly (SSTA) in the equatorial central-eastern Pacific re-entered La Niña conditions in September 2021 and has persisted ever since. Due to the "Matsuno-Gill" effect stimulated by La Niña, as a response, an anomalous low-level anticyclone maintained over the Philippine Sea basin from spring to summer of 2022, resulting in less-than-normal tropical cyclones (TCs) generation in the period. Meanwhile, the warmer surface water from the tropical eastern Indian Ocean to the tropical western Pacific Ocean in this summer was conducive to the westward-extension of the subtropical high over the northwest Pacific Ocean (hereinafter referred to as WPSH), also unfavorable for TC landfall. In addition, during the occurrence of La Niña, the southeasterly winds prevailed over China's offshore area as the TC steering flows, it was conducive to the typhoon moves toward to northwest and the typhoon is easy to move northward.

From 1 January to 31 October, 2022, the Western North Pacific (WNP) and the South China Sea (SCS) have witnessed the generation of 23 TCs, which is 1.1 more than the average number (21.9) of multiple years. Among those 23 TCs, Typhoon Chaba (2203), Tropical Storm Mulan

(2207), Typhoon Ma-on (2209) and Severe Typhoon Muifa (2212) made landfall on the coastal area of China, among which Typhoon Muifa made four times landfall on Zhejiang, Shanghai, Shandong, Liaoning respectively. It is 3.07 less than the average number (7.07) of multiple years.

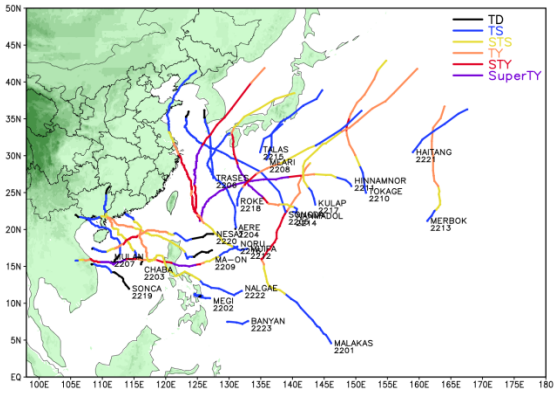


Fig. 1.1 Tracks of TCs over the NWP and the South China Sea from 1 January to 31 October 2022.

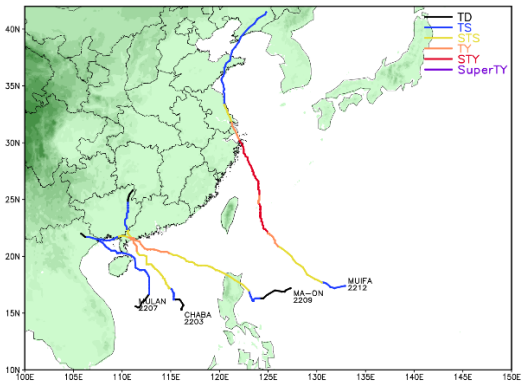


Fig1.2 Tracks of TCs that made landfall over China from 1 January to 31 October 2022.

### 1.1.1 Characteristics of TCs in 2022

The characteristics of typhoons in 2022 are as follows: the source area of typhoons is north and west to the average years, while the number of landing typhoons is less, TCs generated in autumn is more. Another significant feature is the binary typhoons occur frequently, so that the typhoon tracks appear more complex.

**1) Westward and Northward Origins**

Up to October 31th 2022, the averaged genesis location of the 23 TCs is 19.7°N, 134.5°E, which are 3.6 latitude to the north and 1.8 longitude to the west compared with the annual average (16.1°N, 136.3°E, Fig. 1.3).

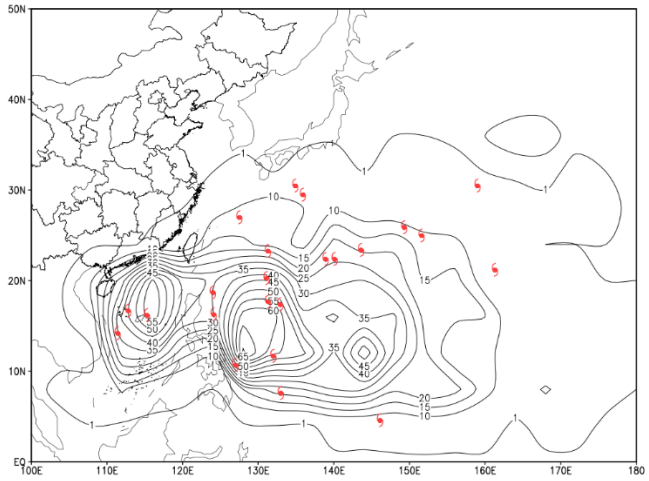


Fig. 1.3 1949-2021 NWP and SCS tropical cyclone source region density distribution (resolution: 2.5°×2.5°) and genesis location of tropical cyclones forming from 1 January to 31 October 2022.

### 2) Slight More TCs Generated, and Frequently in Autumn

Up to 31th October 2022, there were totally 23 TCs generated in the WNP and the South China Sea (SCS), 1.1 more than the average. Except for two TCs generated in April, there are fewer TCs from January to August. There are 12 TCs generated in autumn (September and October), which is 3.5 more than the average number (8.5) of multiple years, making the total number of TCs generated up to now (31th October) exceed the multi-year average by 1.1 (Fig. 1.4).

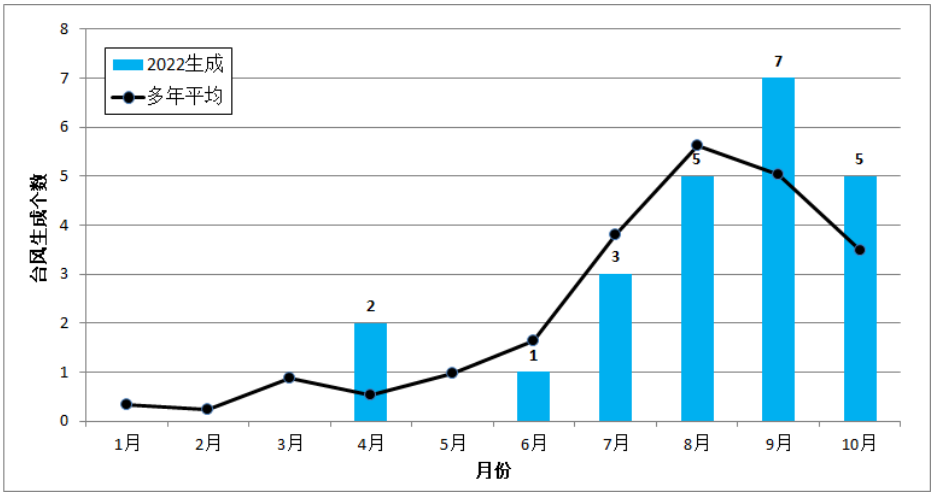


Fig. 1.4 1949-2021 Monthly multi-year average number of TCs (black solid line) and monthly number of TC generation from January to October in 2022 (blue bar).

### 3) Fewer Landfall TCs, and Concentrated Landing Areas

Up to 31th October 2022, 4 TCs made landfall in China, which is 3.07 less than the average number (7.07) of multiple years. And the landing areas are concentrated, there are three TCs landing in western Guangdong, two of which landed in Dianbai in Guangdong Province.

### 4) Frequent Binary Typhoon Activity and Complex Track

Up 31th to October 2022, all of the TCs are accompanied by “binary typhoon” activities, which formed into 13 binary typhoon processes, i.e. Malakas and Megi; Chaba and Aere; Songda and Trases; Mulan and Meari; Ma-on and Tokage; Hinnamnor and TD; Muifa and Merbok; Merbok and Nanmadol; Talas and Noru; Kulap and Roke; Sonca and Nesat; Nesat and Haitang; Nalgae and Banyan. The average binary typhoon activity is significantly higher than multiple years.

Frequent double typhoon activity makes the track complex. The first

landing Typhoon Chaba (2203), after landing in Guangdong, through Guangxi and Hunan, Chaba's residual circulation continued to move northward to affect the central and eastern regions of China, becoming the first typhoon on record that moved from Guangxi to Hunan and Hubei and then move northward to affect Huanghuai, Northeast and other places after landing in Guangdong. Another example is Typhoon Hinnamnor. It moved westward after formation and suddenly turned south near the ocean east of Taiwan. After rotating stagnation, it turned north in a direction of nearly 360°, forming a deep "V" path, which is rare in history.

### 1.1.2 Precipitation of TCs Affecting China

Up to 31th October 2022, a total of 122 rivers in Guangdong, Guangxi, Hainan, Zhejiang, Shandong, Liaoning provinces were flooded by four landing typhoons. Among them, Typhoon Chaba (2103) lead the most destructive damage to the coastal and inland areas. The main characteristics of Chaba precipitation are as follows:

**1) Widely-Ranged Rainfall**

Under the influence of Typhoon Chaba and its weakened low pressure circulation, 17 provinces (districts and cities), including Hainan, Guangdong, Guangxi, Fujian, Hunan, Jiangxi, Hubei, Jiangsu, Anhui, Henan, Shandong, Hebei, Beijing, Tianjin, Liaoning, Jilin and Heilongjiang, have successively experienced extremely rainfall, covering

an area of 34,000, 491,000 and 1,443,000 square kilometers respectively for the accumulative precipitation above 250, 100 and 50mm.

**2) Exceeding Warning Floods and High Level River Network**

Affected by the rainfall caused by Chaba, 93 rivers in the Pearl River basin and Yangtze River basin experienced floods exceeding the warning level with a range of 0.01~5.93m, among which the North River of Guangdong Province witnessed the third Numbered flood of 2022.

### 1.1.3 TCs Affecting China

**1) Typhoon Chaba (2203)**

Tropical storm Chaba formed over the central part of South China Sea at 0000UTC on 30 June 2022, it intensified into a severe tropical storm at 1500UTC, then intensified into a Typhoon at 0000UTC on 2 July. Chaba made landfall over Dianbai, Guangdong Province at 0700UTC on 2 July with the maximum wind speed 35m/s and minimum sea level pressure 965hPa.

After landfall, Chaba continued to move westward and weakened into a severe tropical storm, entered Guangxi Region at evening on 2 July, and weakened into a tropical depression afternoon on 3 July in north part of Guangxi Region. Chaba entered Hunan Province at 0000UTC on 4 July, and continued weakened and moved northward, then the gyre and the residual cloud still affected central-eastern and northeastern China.

Under the impact of Chaba, the accumulated rainfall reached 100–300mm over part of Hainan Island, the central-eastern area of Guangxi, Guangdong, southeastern Fujian, Hunan, western and southern Jiangxi, central part of Hubei, central-eastern Henan, northern Jiangsu and Anhui, central-western Shandong, eastern Hebei, Tianjin, Liaoning, central Jilin and southern Heilongjiang. The accumulated rainfall reached 400-580mm in Guangdong, southwestern Hainan Island, and eastern Guangxi, 695.6mm in Maoming Xinyi Dacheng Town, Guangdong; Daily rainfall at more than 60 stations in Hainan, Guangdong, Guangxi, Hunan, Henan and Anhui reached the level of extremely heavy rain. The daily rainfall at the National Meteorological Observation Station in Sanya, Hainan (421.6mm) exceeded the historical maximum since local meteorological records began.

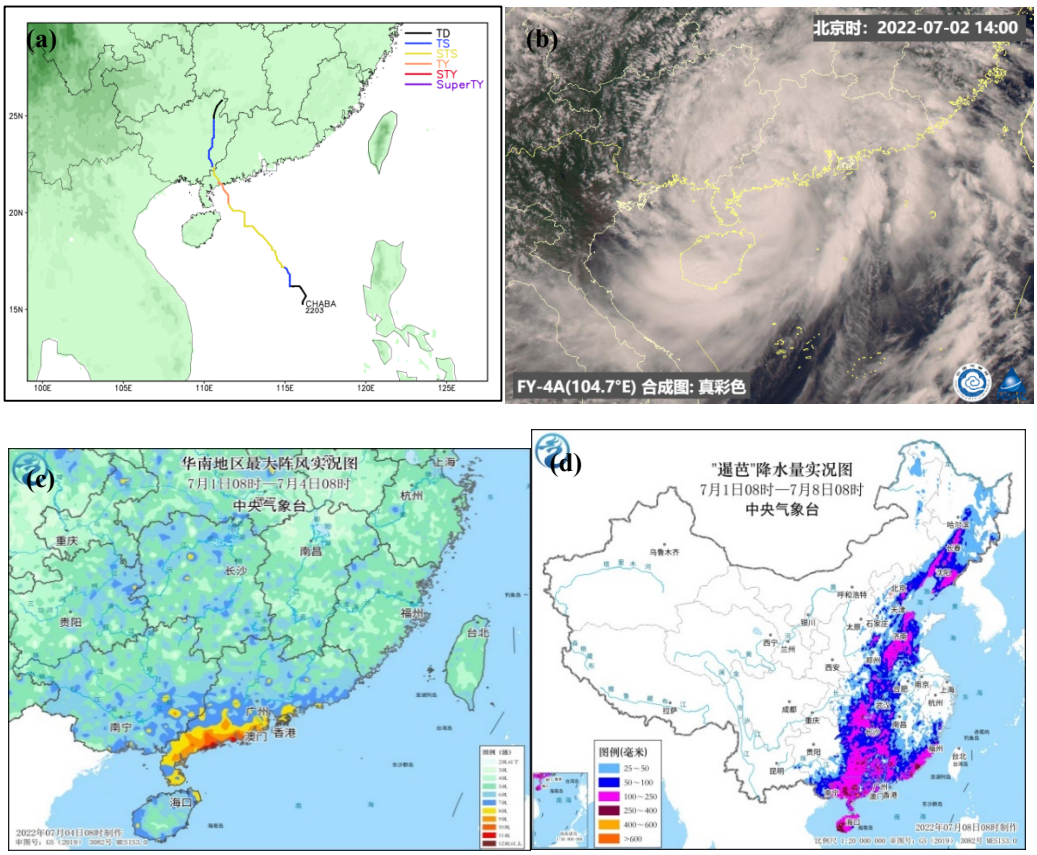


Fig. 1.5 Typhoon Chaba (a)track, (b) FY-4A Satellite image, (c) real-time gust and (d) accumulated rainfall.

### 2) Tropical storm Mulan (2207)

Tropical storm Mulan formed in the central part of the South China Sea at 0200UTC on 9 August and made landfall in the coast of Xuwen, Guangdong Province at 0250UTC on 10 August (23m/s, 992hPa). On 11 August, it made landfall again in northeast Vietnam (18m/s, 998hPa). Then it weakened and disappeared.

Under the impact of Mulan, accumulated rainfall in southwestern Guangdong, southern Guangxi, northwestern Hainan Island reached 100-220mm during 9-10 August, some places of Maoming, Jiangmen and Yangjiang of Guangdong Province reached 250-404mm. There were gales

up to 8-9 scales over the central-western and coastal of Guangxi, eastern Guangdong, northeast coast of Hainan Island and Dongsha, Xisha islands, with some gusts reaching scale 10-12.

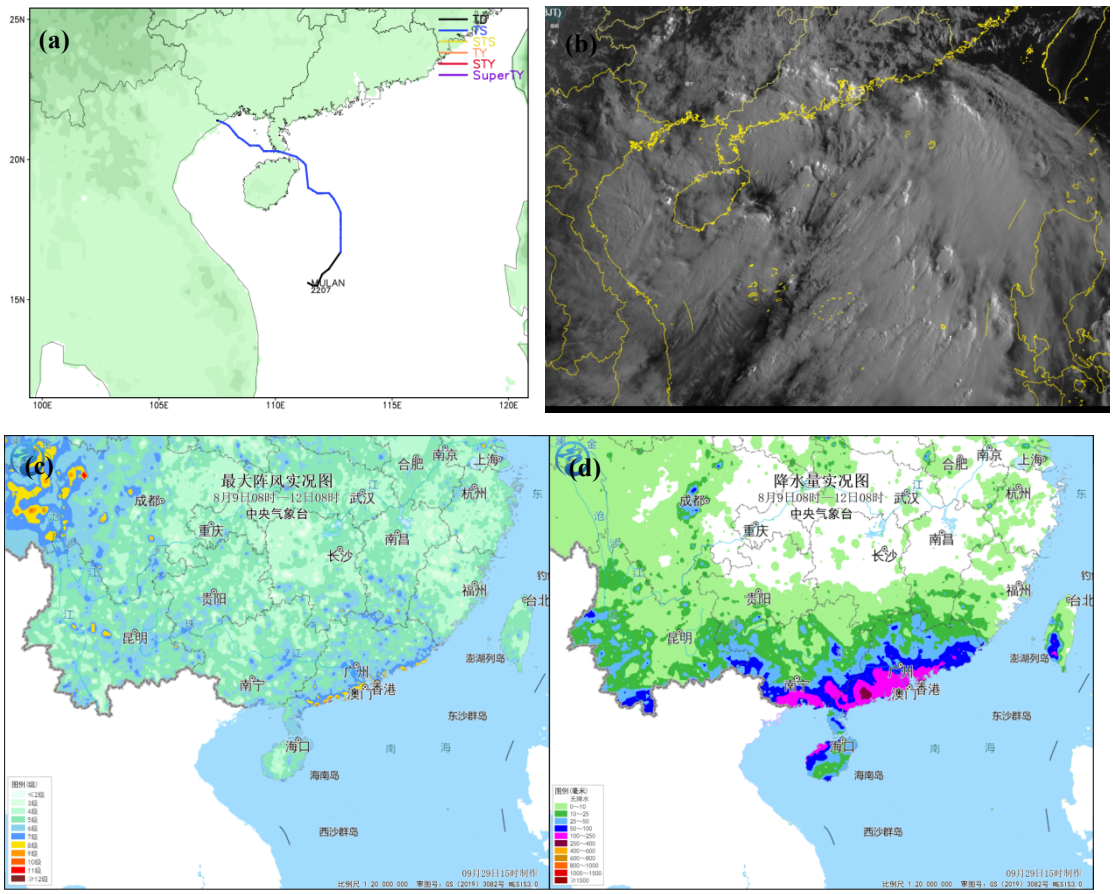


Fig. 1.6 Typhoon Mulan (a)track, (b) FY-4A Satellite image, (c) real-time gust and (d) accumulated rainfall.

### 3) Typhoon Ma-on (2209)

Tropical storm Ma-on formed over sea east of the Philippines at 0600UTC on 21 August and intensified to severe tropical storm at 0000UTC on 23 August. It made landfall in northeastern Luzon (Isabela Province, Philippines, 28m/s, 982hPa) at 0230UTC on 23 August. Then it moved into northeast part of South China Sea and intensified into typhoon at 1200UTC on 24 August. Ma-on made another landfall in the coastal area

of Dianbai, Guangdong (33m/s, 975hPa) at 0230UTC on 25 August, and moved into north part of Beibu Gulf from Guangxi. It made the third landfall in Mong Street, Quang Ninh Province, Vietnam (20m/s, 992hPa) around 0900UTC on 25 August, then weakened and disappeared over Vietnam.

From 24 to 26th August, the accumulated rainfall in southern Guangdong, central-southern Guangxi and Hainan Island was 50-100mm, Jiangmen, Yangjiang, Maoming and Zhanjiang in Guangdong, Fangchenggang and Chongzuo in Guangxi, Haikou, Chengmai, Dongfang and Ledong in Hainan was150-230mm, and 250-344mm in some palces of Fangchenggang in Guangxi. Gusts of 8-9 scale were recorded in some of the above areas, with some gusts reaching 10-12 scale in Yangjiang, Maoming, Jiangmen and Zhuhai in Guangdong, Qinzhou and Fangchenggang in Guangxi, some islands and reefs reaching 13-14scale.

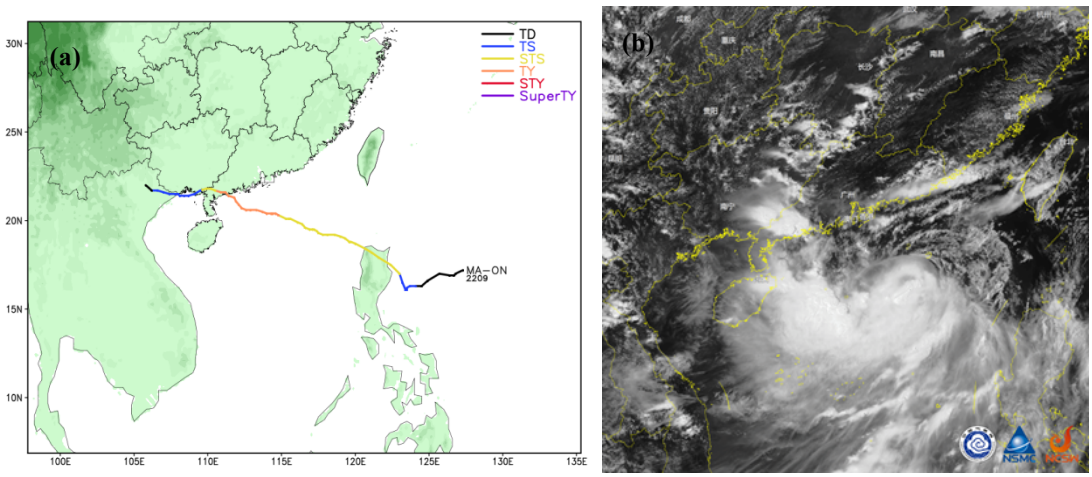

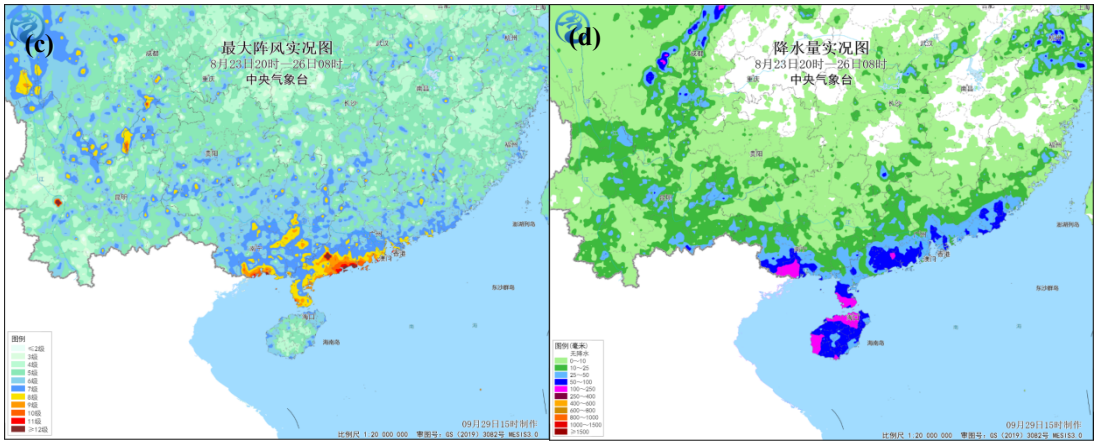


Fig. 1.7 Typhoon Ma-on (a)track, (b) FY-4A Satellite image, (c) real-time gust and (d) accumulated rainfall.

### 4) Super Typhoon Hinnamnor (2211)

Tropical storm Hinnamnor formed over the northwest Pacific Ocean at 0600UTC on 28 August. It intensified into typhoon at 0600UTC on 29 August. At 1800UTC on 29 September, it intensified into super typhoon. At 2100UTC on 1 September, it weakened into severe typhoon over sea east of Taiwan. At 0300UTC on 4 September, it intensified into super typhoon again over the southern part of East China Sea, and at 0800UTC on 5 September, it weakened into severe typhoon. At 1950UTC on 5 September, it made landfall at Juji City, South Gyeongsang, South Korea (45m/s, 950hPa), and then transformed into an extratropical cyclone in the northern part of the Japan Sea.

From 2 to 4 September, under the impact of cloud system around the typhoon Hinnamnor, the accumulated precipitation reached 50-150mm in the eastern and northern parts of Zhejiang, Shanghai, southeastern of Jiangsu and Taiwan Island, reached 200-350mm in Ningbo, Shaoxing in

Zhejiang, 400-461mm locally in the central and northern parts of Taiwan Island. The maximum gust reached scales 6 to 8 in east coast of Fujian, the east coast of Zhejiang, Shanghai, the south of Jiangsu, and the coast of Taiwan Island, and scales 9 to 11 locally.

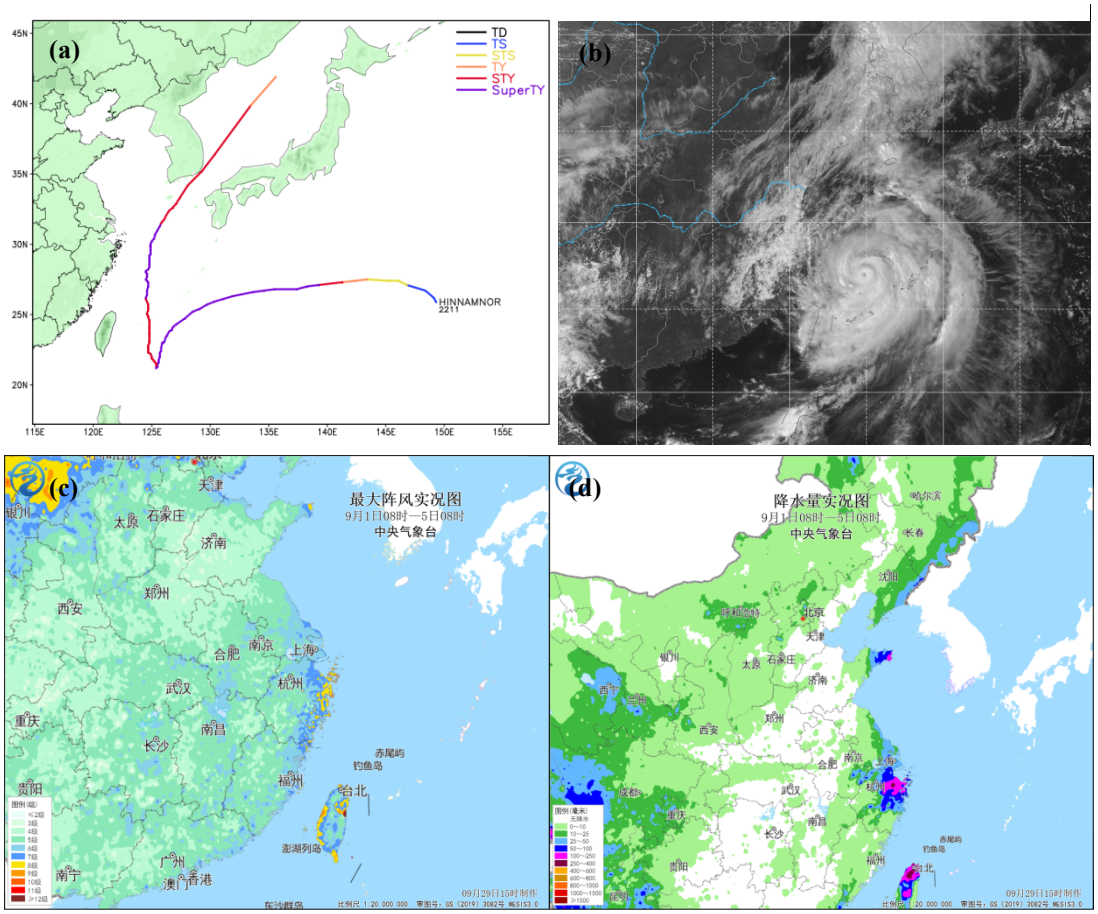


Fig. 1.8 Typhoon Hinnamnor (a)track, (b) FY-4A Satellite image, (c) real-time gust and (d) accumulated rainfall.

### 5) Sever Typhoon Muifa (2212)

Tropical storm Muifa formed over sea east of the Philippines at 0000UTC on 8 September. Then it moved northwestward and intensified into severe typhoon, Muifa maintained the strength for a long time after entering East China Sea. At 1230UTC on the 14 September， it made landfall at the coast of Putuo, Zhoushan in Zhejiang Province (42m/s,

960hPa). Then it moved northwestward and made the second landfall at 1630UTC on 14 September in Fengxian in Shanghai (35m/s, 975hPa). At 1600UTC on 15 September, it made the third landfall at the coast of Laoshan District, Qingdao in Shandong Province (23m/s, 990hPa). It made the fourth landfall in Jinpu New Area, Dalian in Liaoning Province at 0440UTC on 16 September, then it moved northeast and gradually weakened and transformed into an extratropical cyclone.

The strong wind brought by Muifa has a characteristic of wide range, strong intensity and long duration. The maximum gust in eastern Zhejiang, Shanghai, eastern Jiangsu, Shandong Peninsula, eastern Liaoning and some regions reached scales 8 to 10. The maximum gust in the coastal areas of Shanghai, Zhejiang and some islands and reefs reached scales 12 to 15. The maximum gust occurred in Xugong Island, Zhoushan, Zhejiang reached scale 16 (53.6m/s). The accumulated time of gale above scale 12 on the northeastern coast of Zhejiang Province was up to 12 hours.

The accumulated precipitation in the northern and eastern of Zhejiang, Shanghai, the eastern of Jiangsu, Shandong Peninsula, the eastern of Liaoning and the northern of Taiwan Island reached 100-200mm, including 250-500 mm in Shaoxing, Ningbo, Zhoushan in Zhejiang Provence and Qingdao, Yantai in Shandong Province, and 600-707mm in Shangyu, Shengzhou in Shaoxing and Yuyao in Ningbo. The daily rainfall of 23 national meteorological observation stations in Zhejiang (2), Shandong (8),

Liaoning (11) and Jilin (2) has exceeded the extreme value in September, and the daily precipitation of Fushan in Shandong has exceeded the historical extreme value since the establishment of the station.

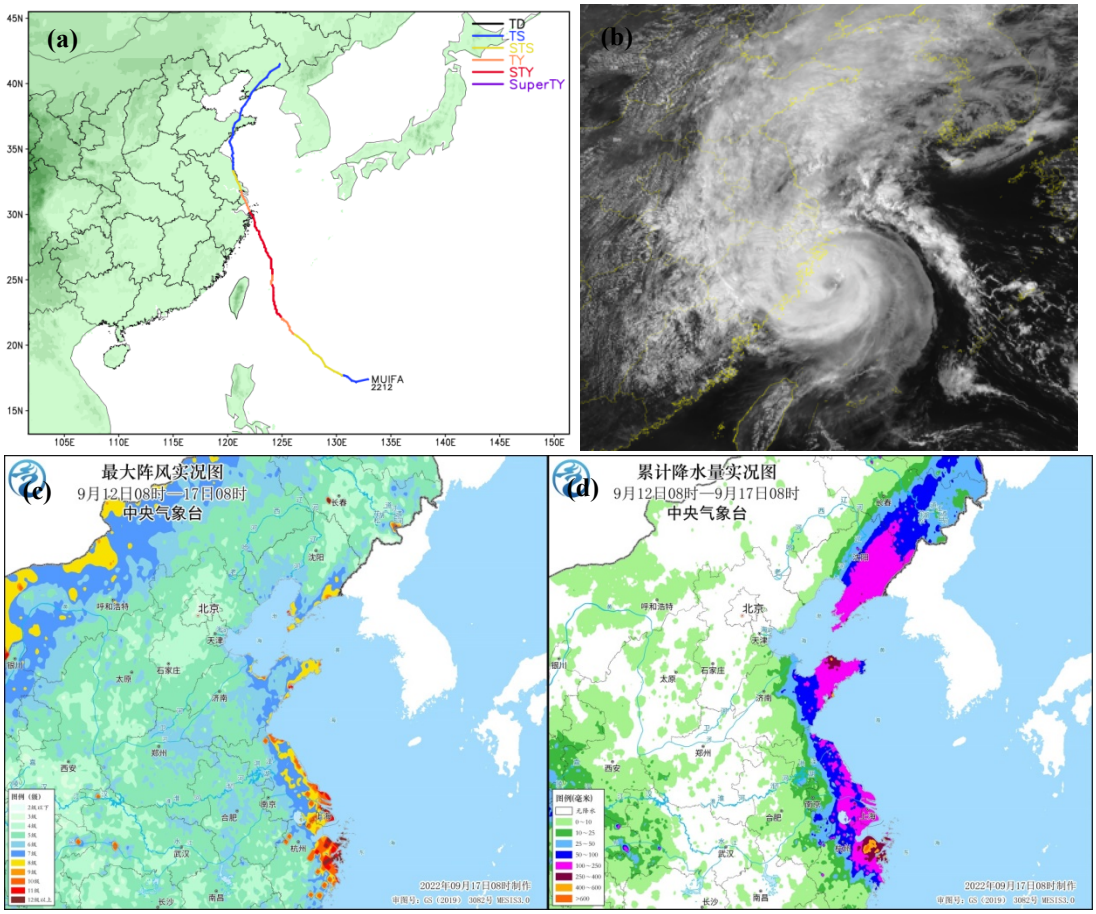


Fig. 1.9 Typhoon Muifa (a)track, (b) FY-4A Satellite image, (c) real-time gust and (d) accumulated rainfall.

### 1.1.4 Climatic Prediction of TCs

In March and May, the National Climate Center carries out seasonal forecasts of TCs in the SCS and the WNP, including the number of TC generation, landfall frequency, possible TCs track and intensity. The main methods are objective method of dynamic-statistical combination and physical mechanism diagnosis.

**1) Annual Prediction of TCs**

In March of 2022, it was predicted that the number of TCs generated in the SCS and the WNP in 2022 would be 22-25, close to or less than the climatology (25, the average during 1991-2020 according to WMO, the same below). Among them, 7-9 TCs would land in China, close to or more than the climatology (7). The overall intensity of the TCs would be medium to weak, and the path of the TCs activity would prevail westward and northwestward, with high possibility of northward landing TCs.

**2) Prediction of TCs during Boreal Summer**

It was expected that there would be 7-10 TCs generated in the SCS and the WNP in the summer of 2022, less than the climatology (11); the number of TCs landing in China would be 4-5, close to the climatology (4.7); the overall strength of typhoon would be medium to weak; and the typhoon activity path would be mainly northwest, with high possibility of northward landing TCs in midsummer.

Observations show that 9 TCs generated in the SCS and the WNP in summer of 2022, 3 of which landed in China. The numbers of genesis and landfall are both less than their climatological mean. The prediction of typhoon genesis frequency is consistent with the observation. However, there is a certain deviation between the prediction and observation for the landing number of TCs. The prediction presents a good prediction skills of

the overall intensity trend and prevailing path of typhoons in summer, being consistent with the northward TC activities affecting China in midsummer.

## 1.2 Socio-Economic Assessment

By 31th October 2022, total 7 TCs affected China, 4 of which made landfalls at the mainland. Loss statistics caused by these TCs read affected population of 4.7 million people in 9 provinces (autonomous region), 3 deaths/missing, evacuated population of 2.0 million people and relocated population of 0.75 million people, collapsed housing of over 800 rooms and damaged housing of over 1,800 rooms, and affected crops of 159,300 hectares and destroyed crops of 11,400 hectares.

On Second July, Typhoon Cempaka (2203) made landfall at Guangdong. It was the first TC that hit China this year, whose was the fourth strength TC since 1991. Typhoon Cempaka demonstrated features of strong wind, heavy rainfall, and wide range of impact. This TC hit Jiangxi, Guangdong, Guangxi, Hainan and totally caused 1.8 million people affected, 3 people dead or missing, 92,000 people evacuated, and 71,000 people relocated. From September 14 to 16, Typhoon Muifa (2212) made landfall on the Chinese mainland four times, causing severe impacts in several eastern coastal provinces. 1.8 million people in Liaoning, Shanghai, Jiangsu, Zhejiang and Shandong were affected, 1.1 million people evacuated, and 556,000 people relocated.

In general, losses caused by typhoon disasters in this year were the lowest since 2000.

**Table 1 Statistics of TCs landfalls and losses in China.**

| TC Name and Number | Landing date, intensity, location | Affected province | Affected population ($10^4$ people) | Dead toll (Person) | Emergency evacuated and relocation population ($10^4$ people) |
|---|---|---|---|---|---|
| Chaba（2203） | 0700UTC, 2 Jul., 35m/s Diannbai, Guangdong | Jiangxi, Guangdong, Guangxi, Hainan | 186.3 | 3 | 16.3 |
| Mulan（2207） | 0250UTC, 10 Aug., 23m/s Xuwen, Guangdong | Guangdong, Guangxi, Hainan | 12.6 | 0 | 7.6 |
| Ma-on（2209） | 0230UTC, 25 Aug., 33m/s Diannbai, Guangdong | Guangdong, Guangxi, Hainan | 53.7 | 0 | 51.2 |
| Hinnamnor（2211） | —— | Shanghai, Jiangsu, Zhejiang | 38.9 | 0 | 36.4 |
| Muifa（2212） | 1230UTC, 14 Sep., 42m/s Zhoushan, Zhejiang<br>1630UTC, 14 Sep., 42m/s Shanghai<br>1600UTC, 15 Sep., 23m/s Qingdao, Shandong<br>0440UTC, 16 Sep., 23m/s | Liaoning, Shanghai, Jiangsu, Zhejiang, Shandong | 177.2 | 0 | 172.8 |

| TC Name and Number | Landing date, intensity, location | Affected province | Affected population ($10^4$ people) | Dead toll (Person) | Emergency evacuated and relocation population ($10^4$ people) |
|---|---|---|---|---|---|
| | Dalian, Liaoning | | | | |
| Noru （2216） | —— | Hainan | 1.6 | 0 | 1.5 |
| Nesat （2220） | —— | Hainan | 3.5 | 0 | 2.7 |
| **Total** | | | 473.8 | 3 | 289.5 |

## 1.3 Regional Cooperation Assessment

### 1.3.1 International Training Course on Typhoon Operations of CMA

The 7th international training courses on tropical cyclone monitoring and forecasting was held by CMA from 24 October to 4 November. There were 172 international participants from 48 countries and regions registered this training course, covering all 6 regions (40 from RA I, 63 from RA II, 3 from RA III, 3 from RA IV, 59 from RA V, 4 from RA VI). This course is aimed at enriching the knowledge and improving the skills of typhoon monitoring and forecasting, and enhancing the understanding of the application of meteorological satellite products and ensemble forecast products, eventually supporting typhoon monitoring and forecasting operations. This training contributes to improve the tropical cyclone monitoring and forecasting services in developing countries, and to create typhoon monitoring and forecasting operations images with Chinese characters.

### 1.3.2 Progress of Tropical Cyclone Research and Review in 2022

Since February 2012, 43 issues of Tropical Cyclone Research and Review (TCRR) have been published. The topics cover tropical cyclone (TC) intensity and structure, TC genesis, TC precipitation, TC climatology, TC review, operational TC forecast verification, TC induced storm surge and flood, and risk management and so on. The published TCRR papers

are attributed to authors from 20 different countries and regions, two-thirds of which are international authors. In order to ensure the quality of the journal, peer-review policy is adopted and two-thirds of the reviewers come from abroad.

To increase the journal impact, TCRR continues to cooperate with the globally familiar publisher, Elsevier BV through KeAi Communications Co., Ltd. In addition, the ScholarOne Manuscripts submission and peer-review system of Clarivate Analytics are adopted. TCRR is now hosted in different locations, including ScienceDirect and KeAi.

Until now, TCRR has been included in three full-text databases: ScienceDirect, DOAJ, and CNKI. All the published papers are easily and freely available. Readers spread over 126 Countries, and the full-text download capacity via ScienceDirect alone in the most recent year exceeded 137000 times. 40 articles published in 2020-2021 have been cited 130 times. TCRR has also been included in the Emerging Sources Citation Index (ESCI), which is like SCI, owned by the Clarivate Analytics. In accordance with Clarivate's recent announcement that all Web of Science Core Collection journals will be granted an Impact Factor in 2023, TCRR is expected to receive first official Impact Factor in June 2023.

# II. Summary of Progress in Priorities supporting Key Research Areas

## 2.1 Discriminating Technique of Typhoon Rapid Intensification Trend Based on Artificial Intelligence

The trend detection of the sudden change of typhoon intensity has always been a difficult issue in typhoon forecast. Artificial intelligence (AI) can implicitly extract the complex features in the images through learning a large number of samples, and it has been widely applied in the meteorological field nowadays. Combining new technologies in the field of AI, National Meteorological Center (NMC) has developed the discriminating technique of typhoon rapid intensification (RI) trend based on satellite cloud images, and explored the application of machine learning in typhoon intensity forecasting.

Constructing large sample annotated datasets using satellite cloud images and best track information, based on the deep residual network (ResNet) model and the long short-term memory (LSTM) model, an automatic and objective method of identifying the trend of typhoon RI was presented through marking and learning the key information on the satellite images of typhoons on the Northwest Pacific and South China Sea from 2005 to 2018. This method introduced the typhoon lifecycle indication and could effectively forecast and identify the trend of typhoon RI. The results of 4 typhoons with RI processes from 2019 to 2021 showed that AI-based

identification typhoon RI trend technique was superior to the traditional subjective intensity prediction method, which has important application values. In addition, by applying the detecting method in analyzing the operational typhoon satellite cloud images in 2022, it was found that AI-based technique could well capture the sudden change tendency of typhoon intensity, and the comprehensive accuracy of independent sample estimation in 2022 reached 84.64%. This technology also provided strong support for the intensity prediction of several rapidly enhanced typhoons in 2022, such as Hinnamnor, Muifa, Nanmadol and Noru (Fig. 2.1).

**Priority Areas Addressed:**

Meteorology

- Enhance the capacity to monitor and forecast typhoon activities particularly in genesis, intensity and structure change.
- Develop and enhance typhoon analysis and forecast technique from short- to long-term.

**Contact Information:**

Member: China

Name of contact for this item: Zhou Guanbo

Telephone: +86-010-68409446

Email: zhougb@cma.gov.cn

## 2.2 Advances in Numerical Modeling of TCs

### 2.2.1 Operational Batch Test of TRANSv1.0

The Typhoon Rapid Refresh Analysis and Nowcasting System (TRANSv1.0), led by Chinese Academy of Meteorological Sciences, was officially put into operation in 2021. TRANSv1.0 integrated series of key technologies such as Ensemble Kalman Filter (EnKF) cycling assimilation technology for radar data, Space-evenly Thinning Method (SETM) for radar wind, and identification for the typhoon targeted assimilation sensitive area, which effectively improved the application capability of radar observation data with high spatial and temporal resolution in typhoon numerical model before typhoon landfall. In 2022, a higher horizontal resolution (1.5km), improved radar data quality control methods, CAMS cloud microphysical parameterization scheme were further tested and integrated in TRANSv1.0. TRANSv1.0 carried out 96 real-time forecasts for four landfalling typhoons affecting China, which operated stably and reliably in the operational environment and it well meets the current typhoon nowcasting needs. During the second level emergency response of Typhoon Muifa (2212) and the third level emergency response of Typhoon Chaba (2203) in 2022, the location, intensity and time of typhoons' landfall were predicted accurately. The high temporal and spatial resolution wind and precipitation forecast products of TRANSv1.0 were used in the national weather consultation, the typhoon encrypted

consultation and the forecast service of Hainan Provincial Meteorological Station.

### 2.2.2 Operational Upgrade of Global Numerical Forecast System CMA-GFS V3.3

On 19th September 2022, CMA-GFS was upgraded to V3.3, which mainly includes: the topography-following height coordinate was upgraded to height-pressure hybrid coordinate, and the upper boundary conditions were adjusted to reduce the forecast bias at higher levels. The tangential linear mode and accompanying mode of the hybrid vertical coordinate dynamic framework were upgraded, the calculation efficiency of tangent and accompanying modes improved and satellite observation data such as Aeolus wind were added. The performance of CMA-GFSV3.3 in the upper level was significantly improved and precipitation forecast score increased with 3%-5% within 3 days. A significant improvement was made in operational stability, and assimilation calculation time was reduced about 50%.

### 2.2.3 Operational Upgrade of Global Ensemble Prediction System CMA-GEPS

On 21th September 2022, CMA-GEPS was upgraded to V1.3 with the deterministic model version is consistent with CMA-GFSV3.3 and the

initial values and model perturbation methods following CMA-GEPSV1.2. The relevant module associated with the different model versions and initial conditions were also upgraded. To enhance the service support capability of the global ensemble forecasting system, new ensemble forecasting products such as tropical cyclone/disturbance track in the North Indian Ocean (Fig. 2.2), tropical cyclone target observation sensitive area, Northeast cold vortex, South China Sea monsoon, high temperature probability and so on were added.

### 2.2.4 Development of Higher Resolution CMA-TYM

The basic version of CMA-TYM with 4.5km horizontal resolution was set up, including the optimization of the model 120h integration stability, the vortex initialization scheme, and the model convective parameterization scheme. The results from 103 samples of 11 typhoons in 2021 and 2022 show that both the mean track forecast error and the mean intensity forecast error are smaller than those of the operational forecast system with 9km resolution (Fig. 2.3).

**Priority Areas Addressed:**

Meteorology

- Enhance the capacity to monitor and forecast typhoon activities particularly in genesis, intensity and structure change.
- Develop and enhance typhoon analysis and forecast technique from short- to long-term.

**Contact Information:**

Member: China

Name of contact for this item: Ma Suhong

Telephone: +86-010-68400467

Email: mash@cma.gov.cn

Name of contact for this item: Li Ying

Telephone: +86-010-58995830

Email: yli@cma.gov.cn

## 2.3 Tropical Cyclone Observation Experiment

### 2.3.1 TC Field Observation Experiments in 2022

The field observation experiments of Typhoons Hinnamnor, Muifa and Noru were carried out from August to September 2022 as in Fig. 2.4(a), by using GPS sounding, boundary layer windprofiler, PARSIVEL disdrometer and automatic weather station. Besides, the radar networking observation was conducted in the experiments of Typhoon Hinnamnor and Typhoon Muifa, and the rocket sounding was successfully carried out in the experiments of Typhoon Noru. As showed in Fig. 2.4(b), the data observed by the six released dropsondes presents well consistency and being identical with the ground-based observation.

### 2.3.2 Validation of Assimilation Technique for Radial Wind Data of Shipborne Radar

Depending on the National Major Scientific Research Instrument Development project "Typhoon Tracking and Detection Instrument" of National Natural Science Foundation of China, an airship is chosen to be the observation platform to make close-in direct observations of TCs in the South China Sea. In order to verify the performance of the shipborne radar assimilation and fusion system, the Typhoon Molave (2020) was taken as a case to carry out an observation simulation system experiment (OSSE) and assimilation simulation observation. It is assumed that the flight

altitude of the airship is 20km, the radar elevation angle of the airship θ=70°, the azimuth resolution of the radar scanning is 1°, the maximum detection distance of radar L=75km and the radial resolution is 150m in the simulation. The radial wind observation of the shipborne radar is obtained by simulation, then the observation simulation assimilation experiment is carried out, some preliminary research results were achieved.

Three experiments were conducted, including nature run, EnKF and noDA experiment. The nature run was the forecast of a TC prediction system developed by Chinese Academy of Meteorological Sciences named Typhoon Regional Assimilation and Predication System (T-RAPS). T-RAPS consists of a TC dynamic initialization (DI) scheme to make the typhoon intensity in the initial field consistent with the measured typhoon intensity, carrying out real-time prediction after years of development. In the nature run, the radial wind observation of shipborne radar was obtained by simulating typhoon wind field with T-RAPS, and then the observation was assimilated. In order to consider the influence of model errors in the assimilation, the initial conditions, model physical process and model resolution of the nature run were artificially different from those of the EnKF experiment.

It was found that the simulation error of the initial position of the typhoon can be significantly reduced by more than 30km compared with the noDA by assimilating the simulated shipborne radar observation (Fig.

2.5). The initial vortex intensity of the typhoon was significantly enhanced, and the minimum sea level pressure is decreased by 12hPa compared with the noDA. The maximum wind speed was increased by 5m/s. In the subsequent deterministic forecast, the minimum sea level pressure of typhoon was close to that of the nature run, and the error decreases by more than 10hPa compared with the noDA. The above experiments have verified the availability of shipborne radar radial wind observation in the typhoon numerical prediction, laying the foundation for the data assimilation from subsequent field observations.

### 2.3.3 Global Marine Products

The National Meteorological Information Centre has collected conventional observations (9684 sites in total) such as buoys and ships from domestic meteorological departments and the Ministry of Natural Resources. Combing with the domestic and international satellite data (30 in total), two global sea surface observation datasets including Global Ocean Observation Hourly Basic Dataset and Chinese Moored Buoy Dataset have been developed through data integration, quality control and evaluation. In addition, a series of multi-source ocean fusion products have also been completed, including global 10 km atmosphere and surface, global 25 km sea surface temperature and sea ice concentration (Table 2.1). The approach is based on fusion analysis algorithms of four-dimensional

ensemble variational hybrid assimilation, local ensemble transformed Kalman filter assimilation, and spatio-temporal multi-scale variation. Those products have been used for monitoring, forecasting and early warning of meteorological disasters such as typhoons.

**Priority Areas Addressed:**

Meteorology

- Enhance the capacity to monitor and forecast typhoon activities particularly in genesis, intensity and structure change.
- Develop and enhance typhoon analysis and forecast technique from short- to long-term.

**Contact Information:**

Member: China

Name of contact for this item: Yu Zifeng

Telephone: +86-021-54896105

Email: yuzf@typhoon.org.cn

Name of contact for this item: Li Ying

Telephone: +86-010-58995830

Email: yli@cma.gov.cn

Name of contact for this item: Zhang Tao

Telephone: +86-010-68407984

Email: zhangt@cma.gov.cn

## 2.4 Space-Air-Ground Collaborative Target Observation and Assimilation to Improve Typhoon Forecast in the South China Sea

Lack of observational data is a great challenge for typhoon track and intensity forecasting. The first Space-Air-Ground collaborative observation experiment was carried out for Typhoon Mulan (2207) over South China Sea between August 8-10, 2022 with cooperation among the Center for Numerical Earth System Prediction of the China Meteorological Administration, the State Key Laboratory of Numerical Simulation of Atmospheric Science and Earth Fluid Dynamics, Institute of Atmospheric Physics, Chinese Academy of Sciences, the Department of Atmospheric and Oceanic Sciences, Fudan University, and the Hong Kong Observatory. Valuable observations were obtained by the Fengyun-4B hyper spectral sounder, airborne down-dropping sounders, and round-trip flat-floating sounders. After assimilation of these observations in CMA-GFS, there was two low centers at 500hPa geopotential height in the analysis field (as shown in Fig. 2.6), while there is only one center in the operational assimilation test (blue curve). The two-centered analytical field seems to be more consistent with the appearance of two connected cloud systems in the region. This suggests that the additional 4B hyper spectral observations contribute to better resolve the relatively weak multi-center character of the low-pressure system in the South China Sea compared with the operation.

For the forecast track of Typhoon Mulan (Fig. 2.7), the 4B GIIRS assimilation forecast starting at 0600UTC on 8 August 2022 was able to capture the irregular motion of Mulan, i.e., first to westward and then northward movement. But the predicted track from the operational forecast was relatively smooth, with the TC basically moving only to the northwest. Meanwhile, with the assimilation of 4B GIIRS data, the TC forecast intensity error for this relatively weak system was reduced by about 11% and the intensity error was reduced during the 36h forecast periods.

**Priority Areas Addressed:**

Meteorology

- Enhance the capacity to monitor and forecast typhoon activities particularly in genesis, intensity and structure change.
- Develop and enhance typhoon analysis and forecast technique from short- to long-term.
- Enhance and provide typhoon forecast guidance based on NWP including ensembles and weather radar related products, such as QPF/QPE.

**Contact Information:**

Member: China

Name of contact for this item: Ma Suhong

Telephone: +86-010-68400467

Email: mash@cma.gov.cn

## 2.5 Establishment of Operational Platform and Data Application of Fengyun Series Satellites

### 2.5.1 Establish the Operational Platform “Fengyun Earth” and Promote the Application of FY-4B and FY-3E Satellite

In 2022, the National Satellite Meteorological Center (NSMC) launched the construction of the full process of whole operations, gathering the development of satellites plans, data processing, improvement of satellite related algorithm, application of satellite products and the construction of application system platform, which named by “Fengyun Earth”. The “Fengyun Earth” operational platform has been established and developed. Until now, “Fengyun Earth” has already been applied in the national meteorological operational intranet, and provide satellite remote sensing monitoring services for meteorological departments at the national, provincial, municipal and county-level.

The “Fengyun Earth” focuses on the design and development of the typhoon monitoring application system based on Fengyun series satellites, covering typhoon track, intensity, structure, wind, rain and the analysis of circulation conditions, with the use of real-time satellite data to test and evaluate the results of numerical forecast model, eventually forming the multi-scale and multi-characteristic analysis products. In the process of developing algorithms for typhoon monitoring, NSMC focuses on the application of new data from FY-4B and FY-3E, and the comprehensive

application capability of satellite remote sensing in typhoon monitoring was improved in conjunction with other Fengyun series satellites. For example, the use of FY-4B satellite for rapid scanning of typhoon areas at the minute scale and the use of the derived wind field at the ocean surface by FY-3E satellite both provided new observations and improved application capability for this year's typhoon monitoring service.

Above mentioned products have been integrated into the "Fengyun Earth" operational platform, and being uses in typhoon monitoring services. By evaluating the feedback from the application in coastal provinces highly affected by typhoons, the platform and the typhoon monitoring products are considered to have the characteristics of high efficiency, easily operation and clear interpretation, which achieving the expected goal of easy to use, good to use, love to use and being useful. In the monitoring of key typhoons affected China, such as Typhoons Muifa and Hinnamnor, NSMC have formed an interactive and jointly service with the National Meteorological Center and coastal provincial departments, and successfully completed the services in this year.

### 2.5.2 Inverted Wind Speed Around TC Center by GNOS-II Sounder of Fengyun-3 Satellite

Global Navigation Satellite System Occultation Sounder (GNOS) is the occultation sounder on board the Fengyun satellite. Since FY-3E, the

GNOS payload has been upgraded to a second-generation, and GNOS-II inherits the occultation detection function of GNOS and at the same time the GNSS Reflectometry (GNSS-R) was added. GNSS-R also uses GNSS signals for remote sensing detection, and determines the nature and state of the target by obtaining the reflection signal of the target to GNSS electromagnetic waves, and ocean remote sensing can obtain information on parameters such as sea surface wind field, roughness, wave height, seawater salinity and sea ice thickness. GNSS-RO and GNSS-R could provide all-day, all-weather observation. GNSS-R can invert the high wind speed near the typhoon's center because navigation satellites emit L-band signals that are not affected by rainfall. Figure 2.8 shows the observation from GNOS-II and inversion sea surface wind of GNSS-R at 28th June 2021 and Figure 2.9 shows the distribution of sea surface wind speed from GNSS-R for Typhoon Malou at 21UTC 26th October. It could be found that inverted wind field could describe the strong wind distribution compared with ECMWF analysis.

### 2.5.3 TC Modeling Experiments Based on Direct Assimilation of FY-4 Data

FY-4B Advanced Geostationary Radiometric Imager (AGRI) was launched in June 2021, added a lower level water vapor channel centered at 7.92μm. The assimilation test of the FY-4B/AGRI water vapor channel

was carried out for Typhoon Malakas (2201). From the assimilation results, the direct assimilation of the FY-4B/AGRI significantly improved the accuracy of the predicted track and intensity of the typhoon (Fig. 2.10). This may be caused by the fact that assimilation improves the distribution of water vapor in the direction of typhoon movement, thus improving the intensity forecast.

In addition, FY4A Geosynchronous Interferometric Infrared Sounder (GIIRS) data assimilation for Typhoon In-Fa (2106) including data thinning, channel selection and O-B statistics was examined through a serial of data assimilation experiments. Results show that the assimilation of FY4A/GIIRS data has a significant influence on the simulation of large-scale atmospheric circulation, and there are obvious different in the warm core structure of 6h forecast. In general, the assimilation of FY4A/GIIRS data has a positive effect on the forecast of Typhoon In-Fa's track (Fig. 2.11).

**Priority Areas Addressed:**

Meteorology

- Enhance the capacity to monitor and forecast typhoon activities particularly in genesis, intensity and structure change.
- Develop and enhance typhoon analysis and forecast technique from short- to long-term.

**Contact Information:**

Member: China

Name of contact for this item: Wang Xin

Telephone: +86-010-68407927

Email: xinwang@cma.gov.cn

Name of contact for this item: Ma Suhong

Telephone: +86-010-68400467

Email: mash@cma.gov.cn

Name of contact for this item: Yu Zifeng

Telephone: +86-021-54896105

Email: yuzf@typhoon.org.cn

## 2.6 Advances in Tropical Cyclone Scientific Research

### 2.6.1 Applied Research of Quantitative Estimation of Tropical Cyclone Precipitation Based on Multi-radar

Calibration error is one of the primary sources of bias in echo intensity measurements by ground-based radar systems. Calibration errors cause data discontinuity between adjacent radars and reduce the effectiveness of the radar system. The Global Precipitation Measurement Ku-band Precipitation Radar (GPM KuPR) has been shown to provide stable long-term observations. In this study, GPM KuPR observations were converted to S-band approximations, which were then matched spatially and temporally with ground-based radar observations. The measurements of stratiform precipitation below the melting layer collected by the KuPR during Typhoon Ampil were compared with those of multiple radar systems in the Yangtze River Delta to determine the deviations in the echo intensity between the KuPR and the ground-based radar systems. The echo intensity data collected by the ground-based radar systems was corrected using the KuPR observations as reference, and the correction results were verified by comparing them with rain gauge observations. It was found that after the correction, the consistency of the echo intensity measurements of the multiple radar systems improved significantly (Fig. 2.12), and the precipitation estimates based on the revised ground-based radar observations were closer to the rain gauge measurements.

### 2.6.2 Tropical Cyclone Size Identification Over the Western North Pacific Using Support Vector Machine and General Regression Neural Network

Identification models of size for Tropical Cyclones (TCs) in the Western North Pacific (WNP) were proposed based on the infrared channel imagery of geostationary meteorological satellites. Several different machine learning algorithms were tested for different TC size parameters, including radius of maximum wind (RMW), radius of 34kt (R34), 50kt (R50) and 64kt (R64). Through evaluation and verification, the trained and optimized support vector machine (SVM) models are proposed for RMW and R34, whereas the general regression neural network (GRNN) models are set up for R50 and R64.

A dataset of the size parameters of 940 TCs above tropical storm intensity during the period 1981–2019 was compiled based on the proposed models. According to the independent-sample evaluations against aircraft observations (1981–1987) and Joint Typhoon Warning Center best track data (2017–2019), the mean absolute errors of R34, R50, R64, and RMW are 54/58, 34/38, NA/21, and 25/25km, respectively (R34 is showed as an example in Fig. 2.13). The corresponding median errors are 39/46, 34/31, NA/17, and 17/19km, respectively. There is an overall slight underestimation of the parameters, which needs to be analyzed and improved in a future study. Despite aircraft observations of TCs in the

WNP having ceased in the late 1980s, this new dataset of TC sizes enables a thorough estimation of wind structures covering a period of 40 years.

### 2.6.3 Analysis on the Deep Convection Activities During TC Genesis Period

Nineteen years (2000-2018) of high-resolution infrared brightness temperature data was adopted to investigate the characteristics of deep convective activities during the genesis and early evolution of TCs in the western North Pacific. It was found that quasi-periodic outbreaks of deep convection are common during TC genesis regardless of the large-scale flow pattern or the magnitude of wind shear. Spatially, deep convection concentrates within 3° of the disturbance center at peak time (when convection is active), and will shrink in coverage and become scattered at trough time (when convection is inactive). At the decay stage deep convection in the central area tends to weaken first. Among the quasi-periodic cycles of deep convection, quasi-diurnal cycles are the most distinct feature, followed by cycles with periods of 10-18 hours. The quasi-diurnal cycles with an early morning peak only account for less than 50%. Statistically the amplitude of deep convection cycles will decrease a bit under shear greater than 9 m/s, and period length in the range of 12-28 hours decreases slowly with the increase in wind shear and will rise slightly when shear is greater than 9 m/s (Fig. 2.14). Besides, genesis does not

necessarily occur at the peak time of coverage in deep convection, and the oscillatory feature is not an effective indicator of genesis acceleration.

### 2.6.4 The Relationship Between the Inner-core Size and the Rainfall Distribution in Landfalling TCs Over China

The TC size is a crucial parameter in determining the destructiveness of a TC, but the relationship between the inner-core size and rainfall distribution in landfalling TCs is little known. This research presents an observational analysis of the relationship between the radius of maximum wind (RMW) and the rainfall in landfalling TCs over China during 2001–2020.It is found that small TCs have higher rainrate with higher axial symmetry than large TCs. Though both small and large TCs have rainfall within a radius of 5 latitudes, the rainfall occurs up to 10 times of the RMW in small TCs compared to within 5 times of the RMW in large TCs. Small TCs have a 6h delayed rainfall decrease compared to large TCs near the landfall (Fig. 2.15). Higher TC intensity may partly contribute to higher rainrate during landfall in smaller TCs than in larger TCs.

### 2.6.5 Downwind Development in a Stationary Band Complex Leading to the TC Secondary Eyewall Formation

This study examined the convection onset in the early stage of Secondary Eyewall Formation (SEF) in the numerically simulated

Typhoon Soudelor (1513). Results show that the convection onset in the SEF region was associated with the organization of a stationary band complex (SBC), which resulted from the outward propagation of inner rainbands and downwind propagation of secondary rainbands, with convection enhanced in the downwind sector of the SBC.

The outward propagation of the inner rainbands involved the mesoscale pressure perturbations-induced unbalanced boundary-layer dynamics, which were responsible for the radial outflow above the boundary layer inflow and the related secondary circulation on the inward side of the rainband. In the downwind propagation, secondary rainbands evolved into stratiform precipitation in the downshear-left quadrant, where a mesoscale descending inflow continuously occurred and transported low equivalent potential temperature ($\theta_e$) and dry air downward and downwind, leading to a decrease in low-level $\theta_e$ on the outward side of the rainband. A balanced state of the cold pool dynamics finally reached in the downwind sector of the SBC between the super gradient-induced vertical wind shear (VWS) and the low-$\theta_e$-induced cold pool, resulting in the convection enhancement. Our results strongly suggest that both the unbalanced dynamics and rainband processes were essential in the early stage of SEF (Fig. 2.16).

### 2.6.6 A Possible Mechanism for the formation of Double Eyewall of Tropical Cyclone

The thermal and dynamic structure evolution of the eyewall of Typhoon Megi (1013) is studied by the numerical simulation using the Advanced Weather Research and Forecasting (ARW-WRF) Model after it landed on Luzon Island and entered the South China Sea. The results show that the original eyewall contracted, fractured, weakened and disappeared due to the increase of friction and the decrease of sea surface entropy flux after its landfall. At the same time, the outer spiral rainbands over the ocean outside the island continued to strengthen and became axisymmetric, causing the formation of a large new eyewall. When the inner core of Typhoon Megi crossed the island and entered the South China Sea, the original eyewall reappeared to form a double eyewall structure (Fig. 2.17). The reappearance of the original eyewall was due to the residual convection inside the vortex and the increased ocean entropy flux.

### 2.6.7 Climate Mechanisms on the Genesis Frequencies Between the Intense and Weak TCs Over Western North Pacific

Previous studies focused on the intense TCs over the western North Pacific (WNP), whose variability is intimately linked to El Niño-Southern Oscillation and extratropical sea surface temperature anomaly (SSTA) in the Pacific. However, weak TCs (WTCs) are more numerous and form

further northwestward. The great number of WTCs and thereby the landfall cases may also cause huge damage to countries in Southeast Asia. Anyway, their modulators are far from fully understood. Our research emphasizes the delayed impact of the early spring North Atlantic tripole SSTA (NAT) on the WTC formation frequency through the “capacitor” effect of sea ice (SIC) and SST in the Barents Sea. A physical-based empirical model is developed for the WTC frequency, and hindcast is performed for the period of 1979-2018. It shows the early spring NAT effectively improves the prediction skill for the WTC frequency, which can be considered as a crucial source of predictability for WTCs.

### 2.6.8 Comparisons of Dominant Factors for TC Genesis Between Different Regions Over the Western North Pacific

Based on the Tropical Cyclone (TC) genesis potential index theory, four key dynamic factors, low-level relative vorticity, middle-level vertical velocity, vertical wind shear, and middle-level vorticity, were diagnosed separately using a Poisson-regression framework. In the three subregions with the most significant TC interdecadal activity in the western North Pacific (WNP), different factors were shown different contributions to TC genesis varying with locations (Fig. 2.18). In short, the TC activities over the southeast quadrant of the WNP (SEWNP) were mainly dominated by the interdecadal Pacific oscillation (IPO), which played an important role

in the decadal variations of dynamical factors. In NWWNP, the TC genesis number exhibited an evident increase caused by an obscure local low-level cyclonic anomaly at the positive IPO phase and a local warm SST anomaly in recent decades. The literature on TC activities in the southern part of South China Sea (SSCS) was less consistent. It was shown that the TCGF decadal variation in the SSCS was mainly affected by the meridional SST gradient. The low SST gradient (SSTG) between the northwestern Pacific warm pool and mid-latitude Pacific warm pool in the southern (or northern) hemisphere, strengthening the cross-equatorial flow and the vertical wind shear over the SCS and the Philippines island, had suppressed TC formation in the SSCS after the 2000s. In addition to common reanalysis data, further analyses with the output of a paleo-reanalysis data EKF400 also confirmed the influence between the SSTG and TC formation in SSCS (Fig. 2.19).

**Priority Areas Addressed:**

Meteorology

- Enhance the capacity to monitor and forecast typhoon activities particularly in genesis, intensity and structure change.

- Develop and enhance typhoon analysis and forecast technique from short- to long-term.

**Contact Information:**

Member: China

Name of contact for this item: Yu Zifeng

Telephone: +86-021-54896105

Email: yuzf@typhoon.org.cn

Name of contact for this item: Li Ying

Telephone: +86-010-58995830

Email: yli@cma.gov.cn

## 2.7 Improvement of Typhoon-related Disaster Management

### 2.7.1 The First National Comprehensive Survey on Natural Disaster Risks

According to the general arrangement of the first national comprehensive natural disaster risk survey, the main part of the survey will be completed in 2022. At present, the national survey of natural resources (geology, Marine), ecological environment, transportation, water conservancy, emergency management, meteorology, earthquake and other ministries has been completed. In terms of the application of the survey results, The State Council Survey Office has issued guidelines and a work plan for the application of the survey results. In accordance with the principle of "conducting survey, applying survey results and getting benefits from these work", the survey mainly focus on improving the basic capacity for disaster prevention and control, emergency management, and serving major national strategies and comprehensive social governance, to guide all industries and regions to make good use of survey data, software system platforms and technical specifications. At present, the survey results have been preliminarily applied in pilot areas and industrial sectors.

### 2.7.2 The Impact Assessment of the Multisource TC Precipitation Data on the Multiscale Urban Pluvial Flood Modeling

Based on automatic weather station (AWS) precipitation observations, radar quantitative precipitation estimates (QPE), and radar fusion data during Typhoon Fitow (1323), the influence of multisource precipitation data on multiscale urban typhoon pluvial food modeling is studied. Taking Shanghai as an example, a simplified 2D hydrodynamic model is applied for flooding simulations. Combining with actual flood incidents reported by the public and soil moisture data, we perform multiscale verifications and determine the applicability of three precipitation datasets in the modeling. The results are as follows: (1) At the city scale, although QPE has higher spatial resolution, these estimates are lower than AWS observations. Radar fusion data have both high accuracy and high spatial resolution. For flood depths above 5cm, the radar fusion precipitation scenario can improve the matching probability by 6%. (2) At the neighborhood scale, the radar fusion precipitation scenario can effectively mitigate the problems of an uneven spatial distribution of stations and a weak QPE to accurately capture pluvial details. (3) Fixed-point assessment shows that different precipitation data have little influence on the temporal characteristics of the modeling result all three types of data can accurately reflect food occurrence times. This work can provide a scientific basis for constructing effective urban pluvial food monitoring systems (Fig. 2.20).

### 2.7.3 Dynamic Pre-assessment Technology of Wind Disaster Risk at School under TC Condition

Differed from the static risk assessment model of the strong wind hazard, this study developed a dynamic pre-assessment technology of wind disaster risk under TC condition. Based on the general survey of hidden risks for the coastal schools in Shanghai and their vulnerability analysis, a dynamic wind disaster risk calculation model was established to form a wind disaster risk pre-assessment product. The research results show that the risk index constructed by the dynamic factor model can pre-evaluate the risk level that is consistent with the actual situation. It is more scientific and reasonable in practical application, and can provide a basis for schools to take timely targeted disaster prevention and mitigation measures.

**Priority Areas Addressed:**

Integrated

- Enhance activities to develop impact-based forecasts and risk-based warning.

DRR

- Provide reliable statistics of mortality and direct disaster economic loss caused by typhoon-related disasters for monitoring the targets of the Typhoon Committee.

- Enhance Members' disaster reduction techniques and management strategies.

**Contact Information:**

Member: China

Name of contact for this item: Yu Zifeng

Telephone: +86-021-54896105

Email: yuzf@typhoon.org.cn

Name of contact for this item: Liu Zhe

Telephone: +86-010-52811138

Email: 76243913@qq.com

## 2.8 Tropical Cyclone Operational Skill Training of CMA

In order to improve the typhoon theoretical level and the typhoon prediction ability of forecasters, the Training Center of CMA held operational training workshop related to typhoon forecast.

From April to May 2022, Training Workshop on Coastal Disastrous Weather was held at the Training Center of CMA in Beijing. This workshop is the first special training workshop focusing on Coastal Disastrous Weather in recent years, which has been widely concerned and welcomed by forecasters in coastal areas. The 37 trainees were all forecasters from coastal areas or areas seriously affected by typhoon disasters.

The main contents of tropical cyclones training workshop contained Operational Progress of Typhoon Weather Forecast, Formation Mechanism of Typhoon Storm Weather, New Technology and Methods of Typhoon Forecast and Waring, Typhoon Forecast Practice, etc. During the courses, a variety of training methods were used, such as teaching, practice, communication and discussions. The training lasted for two weeks.

Through this workshop, the trainees' operational capabilities of multi-source data were improved, meanwhile, they were provided with a large number of forecasting and service ideas for reference.

**Priority Areas Addressed:**

Meteorology

- Enhance and provide typhoon forecast guidance based on NWP including ensembles and weather radar related products, such as QPE/QPF.
- Enhance, in cooperation with TRCG, training activities in accordance with Typhoon Committee forecast competency, knowledge sharing, exchange of latest development and new techniques.

**Contact Information:**

Member: China

Name of contact for this item: Zhang Xin

Telephone: +86-010-68405753

Email: xin09chn@sina.com

# Annexes

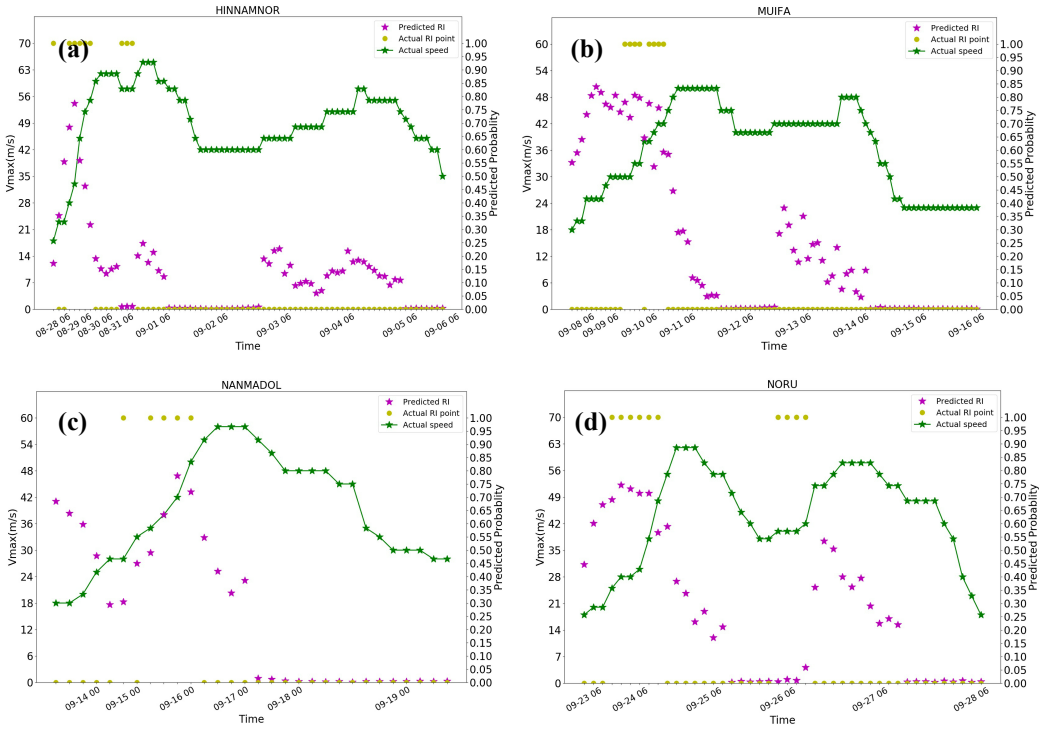


Fig. 2.1 RI probability predicted by the model (purple asterisk) compared with the actual RI probability (yellow dot) and the actual typhoon intensity (green polyline) for: (a) Typhoon Hinnamnor (2211), (b) Typhoon Muifa (2212), (c) Typhoon Nanmadol (2214), and (d) Typhoon Noru (2216).

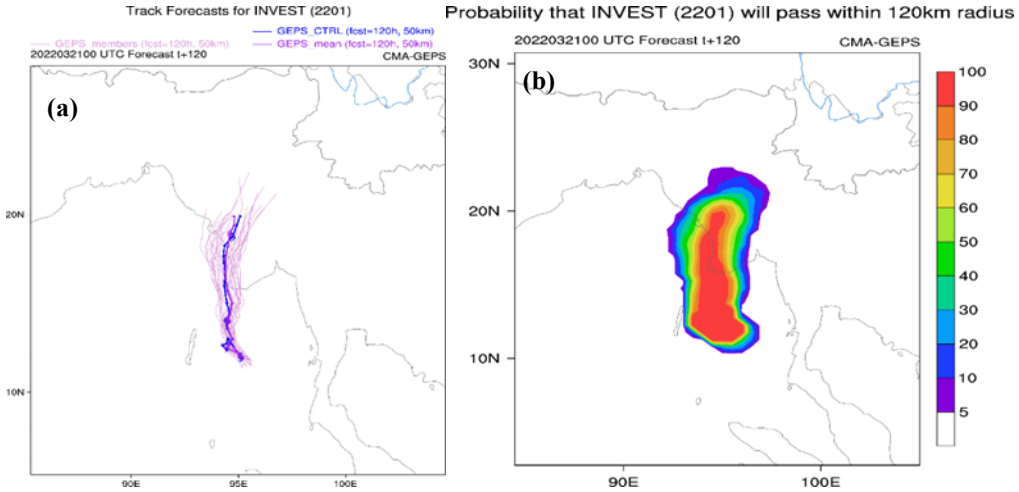


Fig 2.2 (a) CMA-GEPS tracks and (b) strike probability for TC in North Indian Ocean.

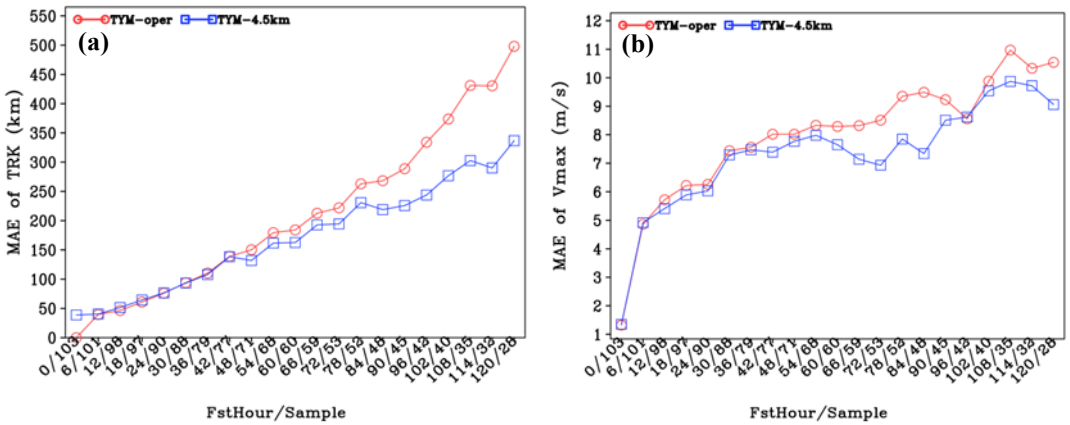


Fig. 2.3 (a) Mean track error and (b) mean intensity error from 103 samples of CMA-TYM in 2021 and 2022.

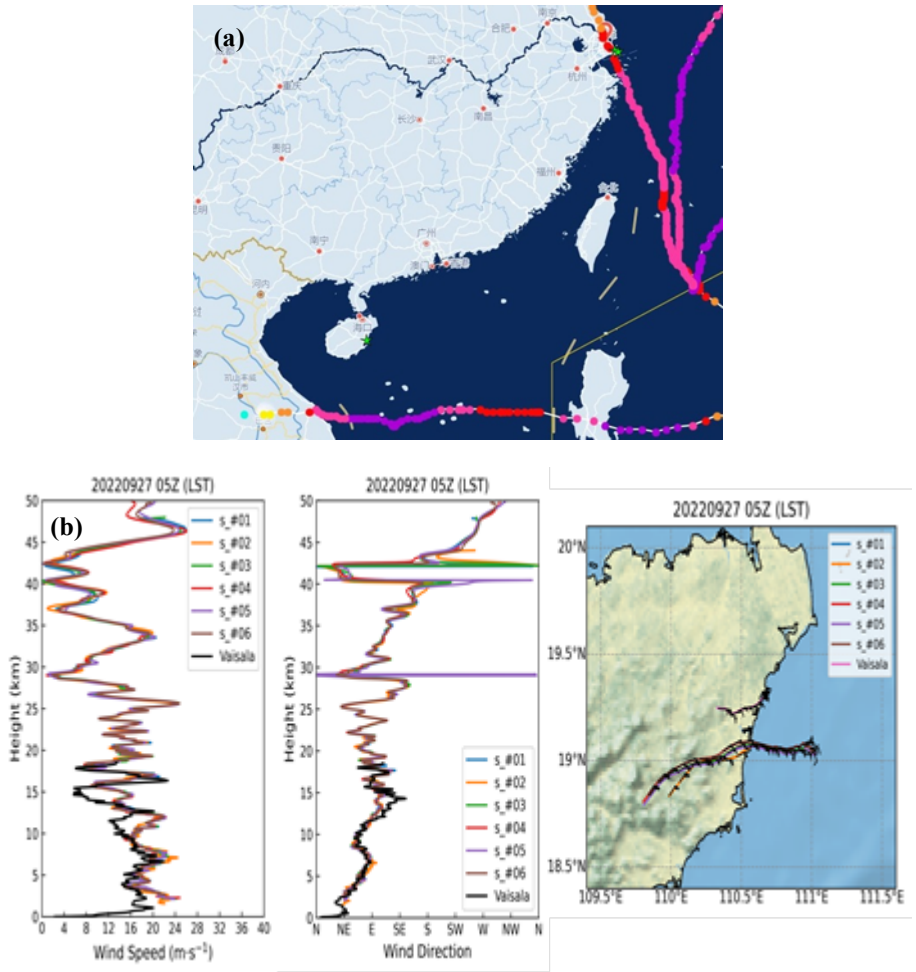


Fig. 2.4 (a) Field experiment locations of Typhoons Hinnamnor, Muifa and Noru (Green pentagram). (b) The wind profiles obtained by the rocket sounding (s_#01-06) and Vaisala MW41 (Vaisala).

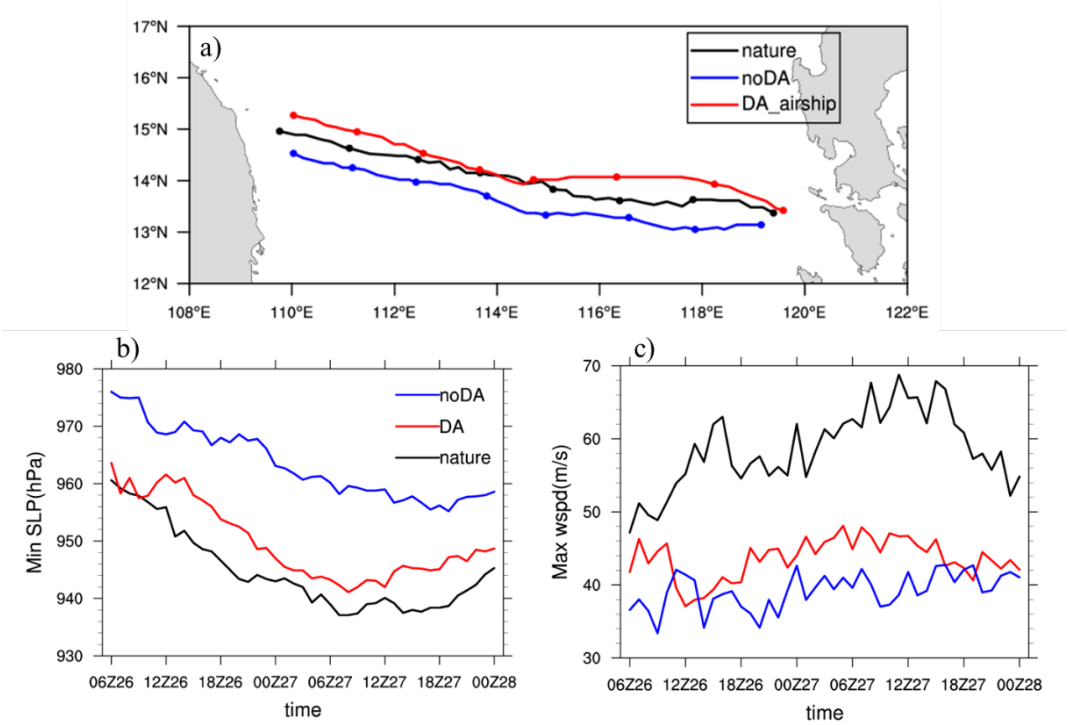


Fig. 2.5 The (a) track, (b) minimum sea-level pressure and (c) maximum surface wind forecast of Typhoon Molave (2018) in EnKF (red curve), noDA (blue curve) and nature run (black curve).

Table2.1 List of Global Marine Products

| Data Type | Dataset | Elements | Update Frequency | Timeliness |
|---|---|---|---|---|
| Observation dataset | Global sea surface observation dataset | 27 hydrometeorological elements such as air pressure, air temperature, dew point temperature, wind direction, wind speed and sea surface temperature | 1 day | 2 days |
| | Chinese moored buoy dataset | 30 meteorological elements such as air pressure, air temperature, relative humidity and wind, and 24 hydrological elements such as sea surface temperature, sea water salinity and waves | 20 minutes | 20 minutes |
| Grid analysis products | Global 10km atmospheric multi-source fusion product | 204 variables such as potential height, temperature, humidity, wind | 6 hours | 4 hours |
| | Global 10km | 2m temperature, specific | 3 hours | 1 hour |

| | | | | |
|---|---|---|---|---|
| | surface multi-source fusion product | humidity, 10m wind | | |
| | Global 25km sea surface temperature multi-source fusion product | sea surface temperature | 1 day | 2 hours |
| | Global 25km sea ice concentration multi-source fusion product | sea ice concentration | 1 day | 12 hours |

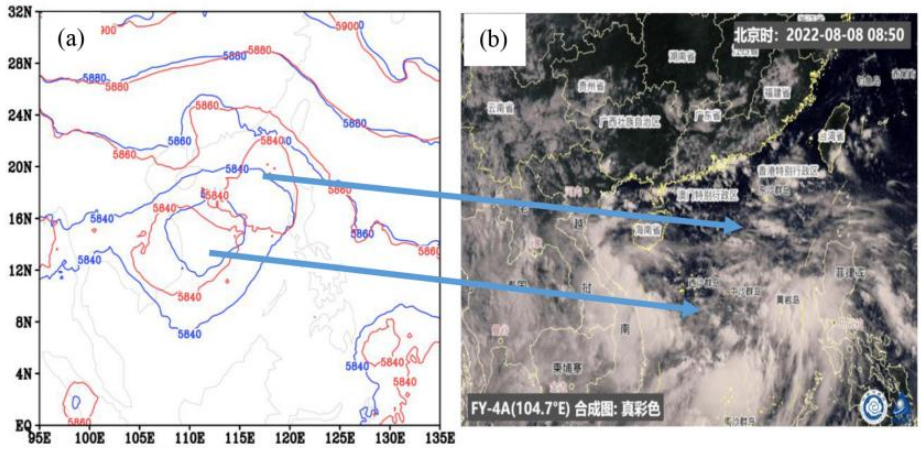


Fig. 2.6 (a) 500hPa geopotential height in the analysis field, blue for the operational analysis and red for the analysis with FY-4B GIIRS data and (b) satellite image from FY-4A at 0050UTC 8 August.

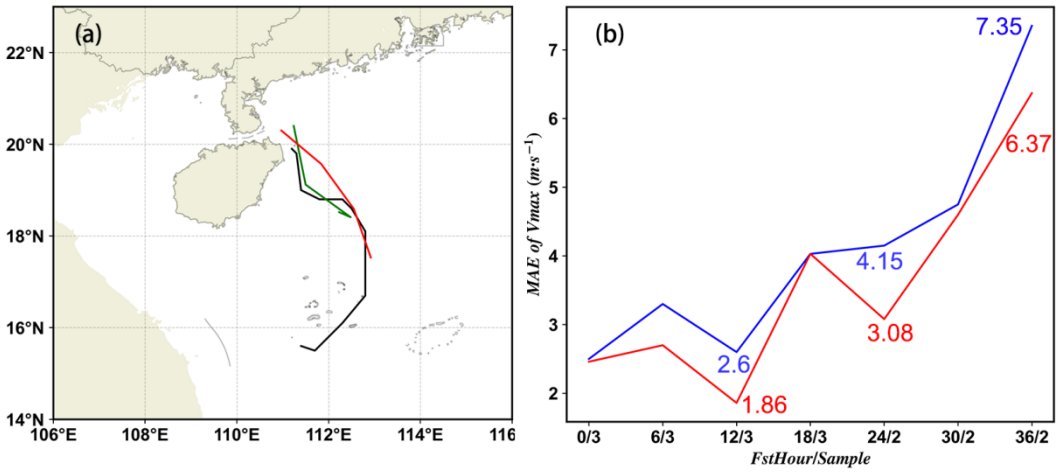


Fig. 2.7 (a) Tracks of Typhoon Mulan for the experiments, black is for best track, red is the operational result; green is for assimilation with FY-4B GIIRS. (b) Errors of TC intensity, blue represents operational result, red is for assimilation with FY-4B GIIRS.

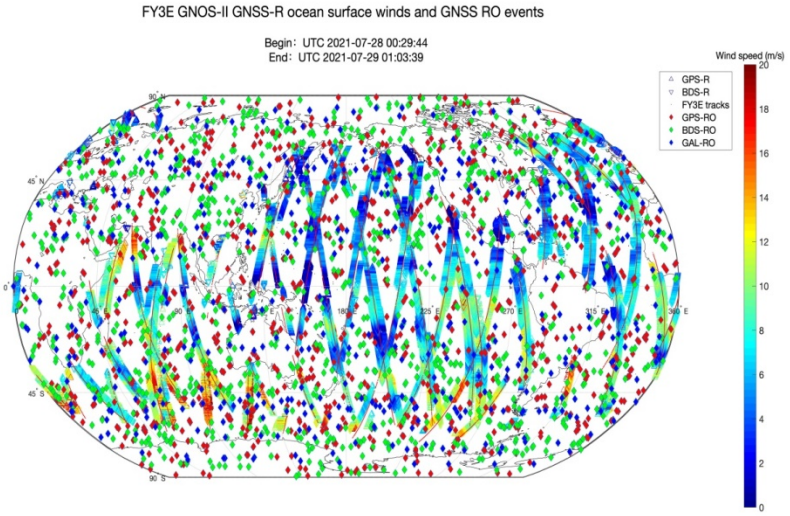


Fig. 2.8 Occultation event observed by FY-3E GNOS and GNSS-R inverted sea surface wind at 28th June 2021.

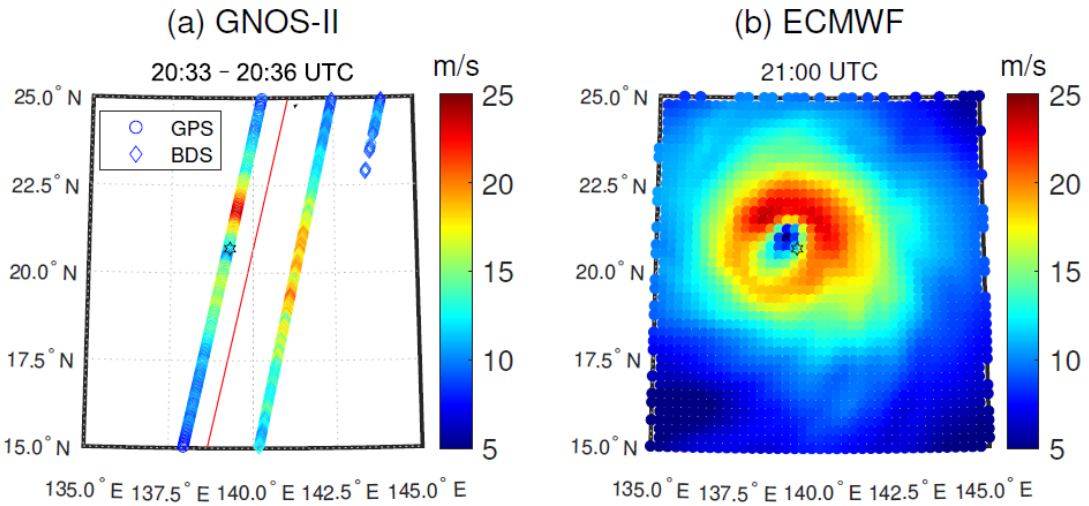


Fig. 2.9 Distribution of sea surface wind speed derived from (a) GNSS-II for Typhoon Malou at 21UTC 26th October and the result of (b) ECMWF.

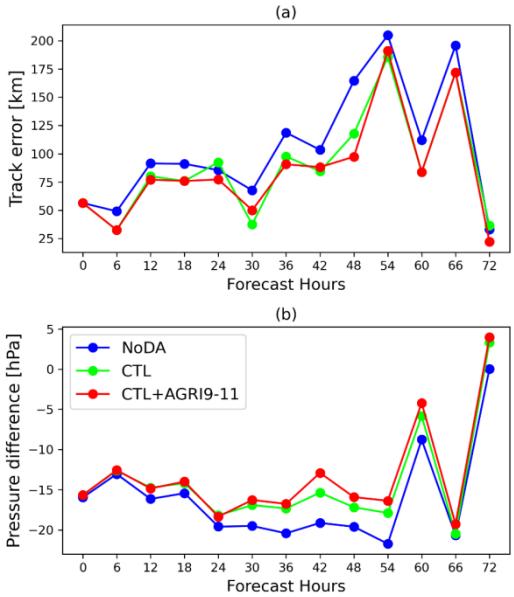


Fig. 2.10 Forecast errors in the (a) track and (b) intensity of Typhoon Malakas (2201) from different forecast tests.

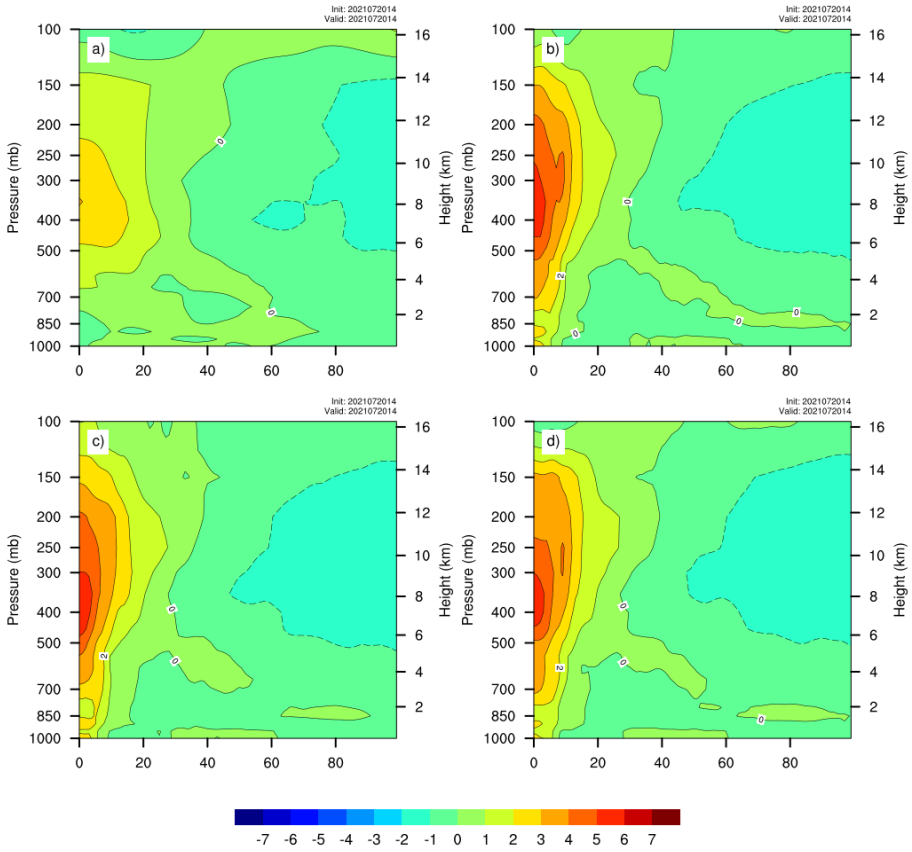


Fig. 2.11 Simulated warm core structures of Typhoon In-Fa from different experiments compared with the ERA5 reanalysis at 0600UTC on 20 July 2021. (a) ERA5 reanalysis, (b) NoDA, (c) CTRL, and (d) GIIRS.

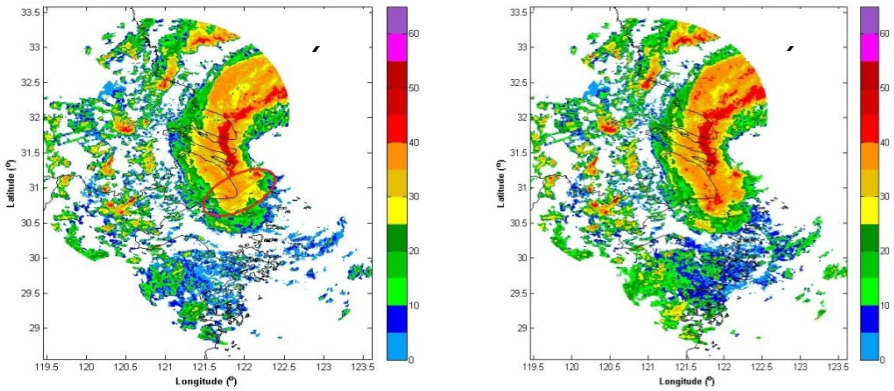


Fig. 2.12 Three-radar (Zhoushan, Qingpu and Nantong) mosaic of the echo intensity of Typhoon Ampil (1810) at 1-km height (a) before and (b) after the correction at 0230UTC at 22 July, 2018.

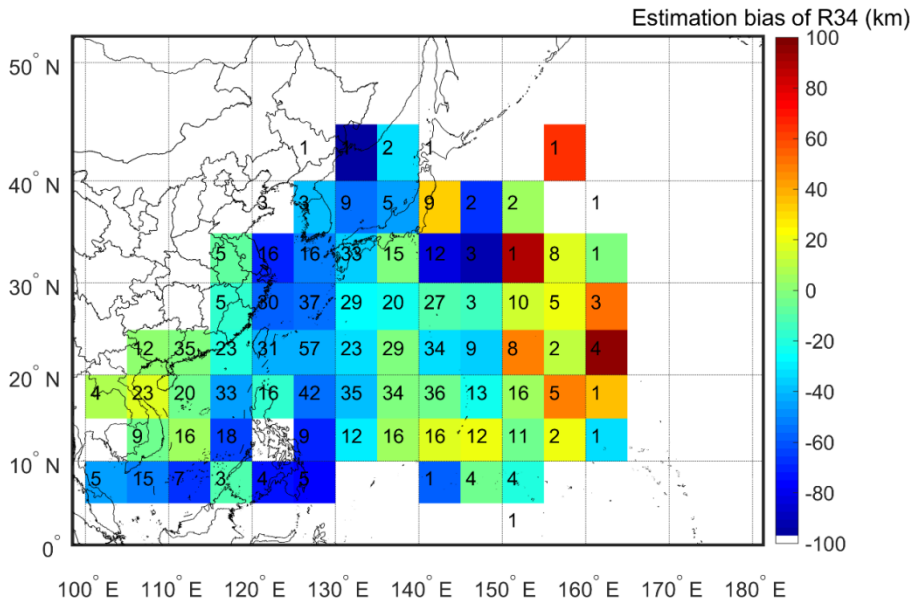


Fig. 2.13 Spatial distribution of estimation bias of R34 compared with the JTWC best track data in the WNP between 2017 and 2019 (1035 samples). The number in each grid is the sample size.

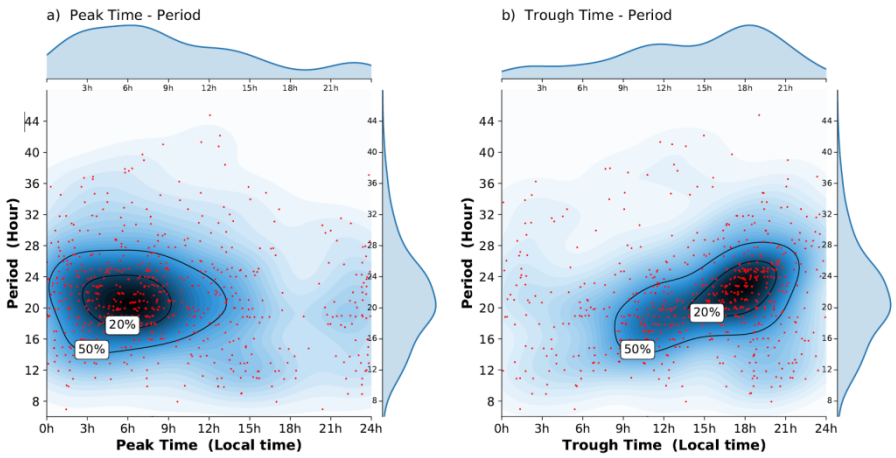


Fig. 2.14 The probability distribution of (a) peak and (b) trough time along with period length of the deep convection cycles.

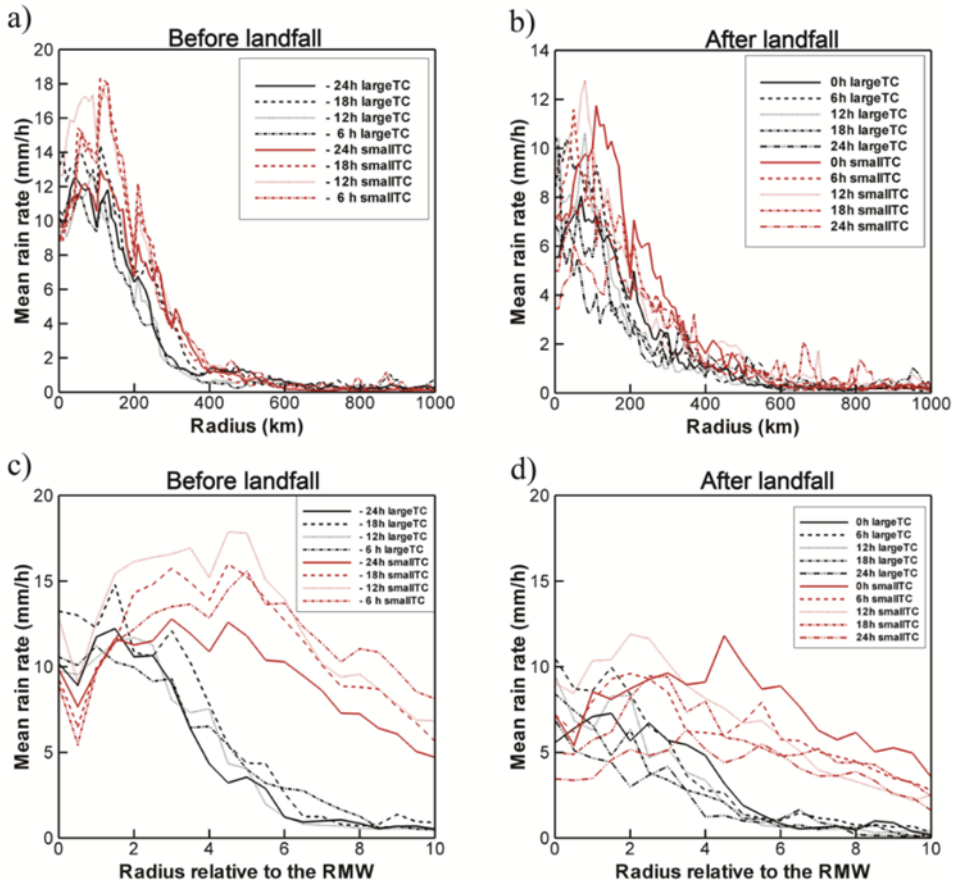


Fig. 2.15 Radial distributions of axisymmetric rainrate (mm $h^{-1}$) from -24 to 24h, composited for large TCs (black) and small TCs (red). The x-axis in (a) and (b) is the physical radius (km) from the TC center and in (c) and (d) is the radius normalized by the RMW.

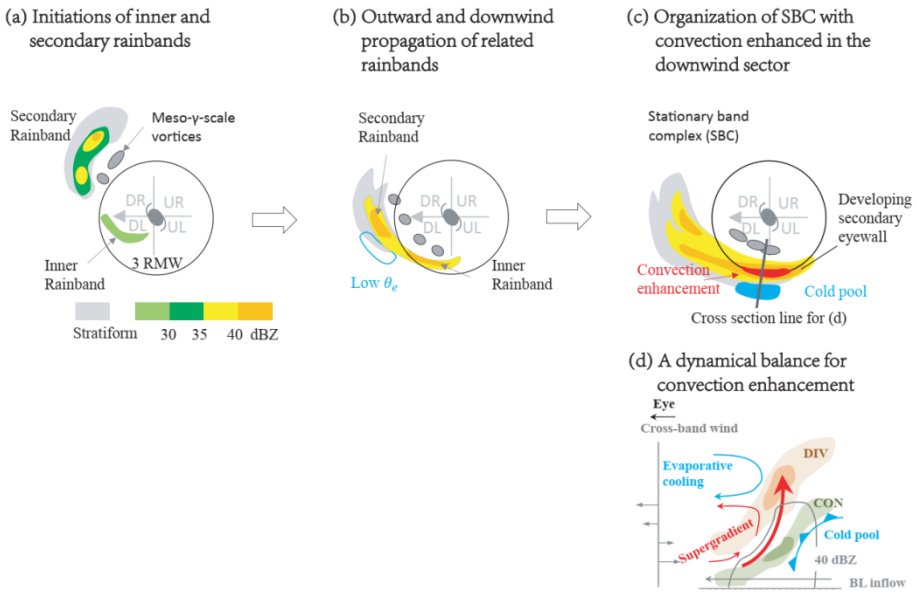


Fig. 2.16 The interaction between inner and second rainbands leads to the convection onset in the early stage of secondary eyewall formation.

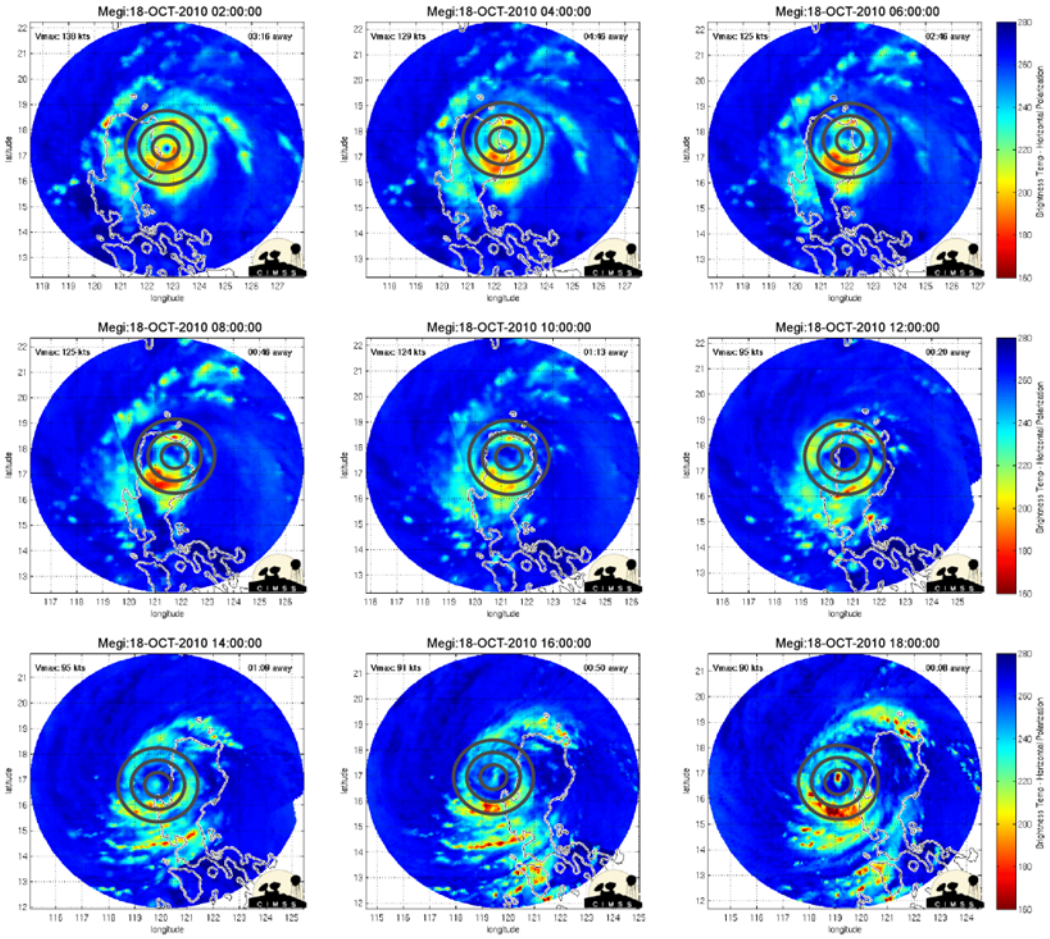


Fig. 2.17 The MIMIC-IR brightness temperature (shading, unit: K) at given times for Typhoon Megi (1013).

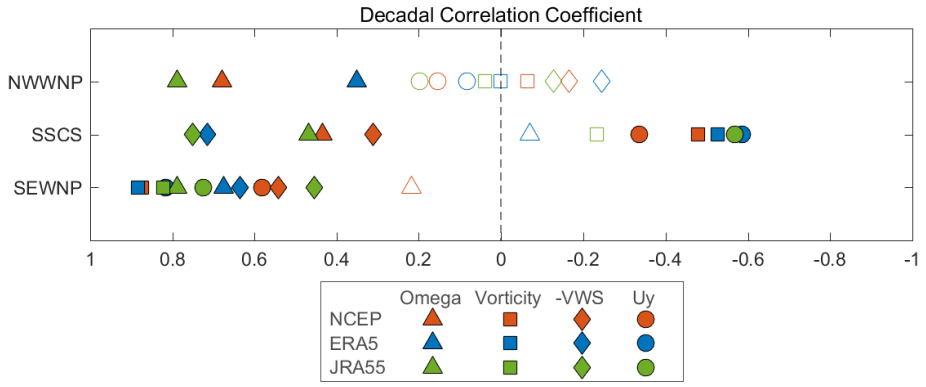


Fig. 2.18 The decadal correlation coefficient between observed TCGF with the results of a possion-regression framework in three sub-regions. The black border indicates the correlation coefficient is statistically significant at the 95% confidence level.

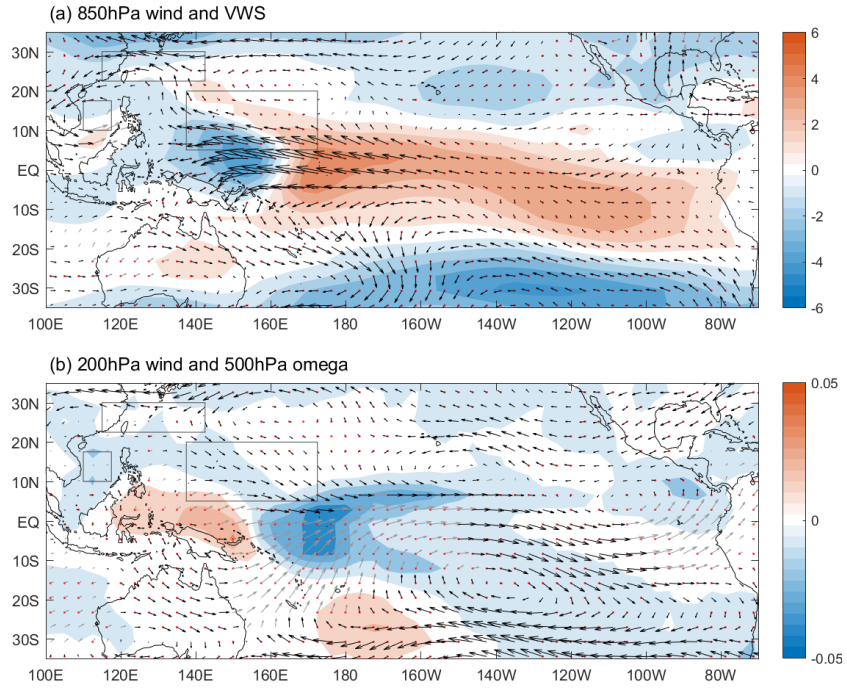


Fig. 2.19 The regressed fields of EKF400 paleo-reanalysis during 1850 to 1950 with respect to the reversed (negative) South-SSTG index: (a) 850hPa horizontal winds and vertical wind shear between 200hPa and 850hPa (shaded; m/s), (b) 200hPa horizontal winds (vectors; m/s) and 500hPa vertical pressure velocity (shaded; Pa/s). Areas that are statistically significant at the 95% confidence level are denoted by red dots based on the Student's t-test. The black box indicates the TCGF in the sub-region shows a significant decadal variation.

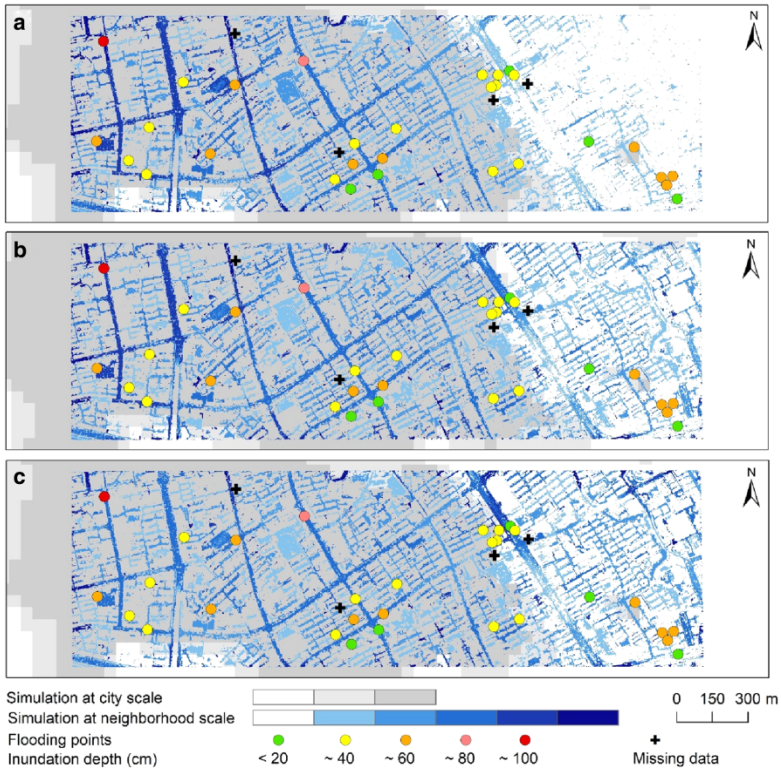


Fig. 2.20 Observed flooding points and pluvial flood inundation maps under three rainfall scenarios in the studied neighborhood of Shanghai during Typhoon Fitow (1323). (a) Scenario of station observations; (b) scenario of radar fusion data; (c) scenario of radar quantitative precipitation estimates (QPE).